

1 **Elevated aerosol layers modify the O₂-O₂ absorption measured by ground-based**
2 **MAX-DOAS**

3

4 Ivan Ortega^{1,2}, Larry Berg³, Rich Ferrare⁴, Johnathan Hair⁴, Chris Hostetler⁴, and Rainer Volkamer^{1,2}

5

6¹Department of Chemistry and Biochemistry, University of Colorado, Boulder, CO, USA

7²Cooperative Institute for Research in Environmental Sciences (CIRES), Boulder, CO, USA

8³Pacific Northwest National Laboratory, Richland, WA, USA

9⁴NASA Langley Research Center, Hampton, VA, USA

10

11 *Revised manuscript in response to the reviewer comments*

12 *Prepared for publication in the Journal of Quantitative Spectroscopy and Radiative Transfer*

13 *Last edited 13 Feb 2015*

14

15 *Corresponding Author:* Rainer Volkamer, 215 UCB, Boulder, CO 80309; Tel: +1 303-492-1843;

16 email: rainer.volkmmer@colorado.edu

17

18 **Abstract**

19

20 The oxygen collisional complex (O_2 - O_2 , or O_4) is a greenhouse gas, and a calibration trace gas used to
21 infer aerosol and cloud properties by Differential Optical Absorption Spectroscopy (DOAS). Recent
22 reports suggest the need for an O_4 correction factor (CF_{O_4}) when comparing simulated and measured O_4
23 differential slant column densities (dSCD) by passive DOAS. We investigate the sensitivity of O_4
24 dSCD simulations at ultraviolet (360 nm) and visible (477 nm) wavelengths towards separately
25 measured aerosol extinction profiles. Measurements were conducted by the University of Colorado
26 2D-MAX-DOAS instrument and NASA's multispectral High Spectral Resolution Lidar (HSRL-2)
27 during the Two Column Aerosol Project (TCAP) at Cape Cod, MA in July 2012. During two case study
28 days with (1) high aerosol load (17 July, AOD ~ 0.35 at 477 nm), and (2) near molecular scattering
29 conditions (22 July, AOD < 0.10 at 477 nm) the measured and calculated O_4 dSCDs agreed within
30 $6.4\pm 0.4\%$ (360 nm) and $4.7\pm 0.6\%$ (477 nm) if the HSRL-2 profiles were used as input to the
31 calculations. However, if in the calculations the aerosol is confined to the surface layer (while keeping
32 AOD constant) we find $0.53 < CF_{O_4} < 0.75$, similar to previously reported CF_{O_4} . Our results suggest that
33 elevated aerosol layers, unless accounted for, can cause negative bias in the simulated O_4 dSCDs that
34 can explain CF_{O_4} . The air density and aerosol profile aloft needs to be taken into account when
35 interpreting the O_4 from ground-based MAX-DOAS. Opportunities to identify and better characterize
36 these layers are also discussed.

37

38 Keywords: DOAS, oxygen collisional complex (O_4), O_4 correction factor (CF_{O_4}), aerosol extinction
39 profiles, and elevated aerosol layers.

40

41 **1. Introduction**

42

43 The collision-induced absorption of oxygen (O_2 - O_2 , or O_4) absorbs solar radiation at multiple bands
44 throughout the ultraviolet (UV), visible and near-infrared regions of the electromagnetic spectrum^[1,2].
45 O_2 - O_2 has no bound state at atmospherically relevant temperatures, and its concentration in the
46 atmosphere is proportional to the square of the oxygen concentration. Hence it can be predicted with
47 little error ($< 0.1\%$) if the temperature and pressure profiles are known^[2]. Analysis of the strong
48 absorption bands of O_4 provides a unique way to characterize how clouds and aerosols modify the
49 photon trajectories, therefore providing information about cloud-top pressure, effective cloud coverage,
50 and aerosol optical properties. In particular, O_4 is being used extensively as an atmospheric reference

51gas in Differential Optical Absorption Spectroscopy (DOAS) applications, including Multi Axis DOAS
52(MAX-DOAS)^[3-6], airborne MAX-DOAS^[7-9], in-situ DOAS instruments^[2,10], and satellites^[11]. Since
53most of the O₄ is located below 4 km, the analysis of O₄ is particularly useful to infer aerosol and cloud
54properties in the lowermost part of the troposphere.

55

56Trace gas profiles derived from passive DOAS techniques, i.e., MAX-DOAS and airborne
57MAX-DOAS, require aerosol extinction profiles as prerequisite information in radiative transfer
58models (RTM). The vertical sensitivity of the measurements to perturbations in the species of interest
59is quantified by the weighting functions, which for optically thin absorbers such as O₄ are the same as
60the box-air mass factor (bAMF)^[12]. The weighting functions are calculated with RTMs by the ratio of
61the partial slant column density (SCD) to the partial vertical column density (VCD) contained in an
62atmospheric layer. Retrieval algorithms based on nonlinear inversion such as optimal estimation need
63the weighting functions^[13]. If the photon path trajectory in the RTM is well-constrained by knowledge
64of the aerosol extinction, then the error in the weighting functions decreases; consequently, the final
65error of the trace gas inversion also decreases. By contrast, assumptions about aerosol extinction
66profiles can lead to considerable errors. In this context, O₄ observations are important because they
67yield information about the extinction profiles^[3,4]. Over the past few years, many ground-based
68MAX-DOAS observations have reported O₄ dSCDs that exceed those simulated by RTM. An O₄
69correction factor (CF_{O₄}) was applied to improve the correlation of simulated and measured O₄
70differential AMF (dAMF or differential SCD, dSCD; differential with regards to the amount contained
71in the reference spectrum)^[5,14-18]. The cause of this CF_{O₄} is currently not understood. Recent airborne
72and direct-sun DOAS testing of O₄ dSCDs did not find a need for CF_{O₄}^[9,19]. However, the CF_{O₄} values
73reported by ground-based MAX-DOAS vary between different studies, see Table 1, and CF_{O₄} is
74consistently needed at low AOD (< 0.2 at 360 nm)^[5,14] and/or at high AOD (up to 1.5 at 477 nm)^[15-18].
75Past MAX-DOAS studies that needed CF_{O₄} have either lacked independent measurements of vertically
76resolved extinction profiles, and/or made simplifying assumptions about the aerosol extinction profiles,
77i.e., confining aerosols to the near the surface (within the boundary layer (BL), see Table 1).

78

79Table 1: Previous ground-based MAX-DOAS using the CF_{O₄}

Reference	Wavelength (nm)	AOD	Aerosol Profile information ^a	CF _{O₄}
Wagner et al. [14]	360	0.1 – 0.2	NO ^b	~ 0.78

Clémer et al. [5]	360, 477, 577, 630	< 0.15 (360 nm)	NO ^c	0.75
Irie et al. [15]	360, 477	0.1 – 1.0	NO ^d	0.75
Vlemmix et al. [16]	477	0.1 – 0.8	NO ^e	0.80
Zieger et al. [17]	360, 477	0.1 – 0.8	Qualitative ^f	~ 0.80 ^g
Irie et al. [18]	476	0.1 – 1.5	Qualitative ^h	~ 0.83 ⁱ

80^aIndicating whether highly resolved aerosol extinction profiles (BL and free troposphere) were
81available and/or used in the simulation of O₄. ^bAerosol profile approximated as box-profile, i.e.,
82constant extinction between the surface and 1 km. ^cCF_{O4} was determined using elevation angles of 15°
83and 30°; aerosol profile assumption: exponential decrease with a scale-height of 0.5 km, AOD as
84measured by a co-located Sun photometer. ^dAerosol extinction retrieval; assumes exponential decrease
85in the lowest 1 km. ^eSimilar approach as in [5]. ^fRaman lidar (355 nm); assumes a backscatter to
86extinction ratio between 60 m and 750 m; above 750 m the lidar ratio was determined and multiplied
87with the backscatter signal to obtain extinction profiles (200 m resolution). ^gAverage CF_{O4} applied to
88four participating MAX-DOAS during the CINDI campaign. ^hAerosol extinction in the BL was
89inferred by lidar, assuming a constant lidar ratio; lidar extinctions in the BL were compared with
90independent in-situ and MAX-DOAS retrievals. MAX-DOAS extinctions profiles were retrieved by
91modifying profile shapes in 1 km thick layers below 3 km constrained by partial AODs. ⁱCalculated
92with the empirical off-axis scan dependent CF_{O4} to a set of elevation angles (<= 10°); in this case 10°.
93

94Uncertainties in the temperature and pressure dependencies of O₄ cross sections had been suggested as
95possible causes for the CF_{O4} [5,14]. Recently, laboratory measurements of the O₄ absorption cross
96sections have quantified the temperature dependence of the spectral band shape for a variety of bands
97at ultraviolet and visible wavelengths (Thalman and Volkamer [2]). The O₄ bands at 360 and 477 nm
98have further been reproduced from field observations in a Rayleigh atmosphere within narrow error
99bounds (< 3 % error)[19]. This error is significantly smaller than the 25 ± 10% differences reported in
100the literature (see Table 1). Furthermore, Volkamer et al. [9] compared modeled and measured O₄
101dSCDs from airborne MAX-DOAS, and reconciled the inferred aerosol extinction profile with
102independent aerosol extinction profiles retrieved by High Spectral Resolution LIDAR (HSRL) in the
103presence and absence of aerosol. They did not need CF_{O4} different from unity over the full range of
104altitudes probed (0 - 14.5 km). Some recent evaluations of ground-based MAX-DOAS have used
105qualitative information about aerosol vertical distributions (e.g., Irie et al. [18]; Remmers and Wagner
106[20]). To our knowledge only airborne MAX-DOAS has been evaluated using quantitative
107vertically-resolved aerosol profiles [9]. In this work, we study the effect of simplifying assumptions
108about aerosol profiles on O₄ dSCDs, and assess the validity of these assumptions using independent
109measurements of highly-resolved aerosol extinction profiles using the data from NASA's HSRL-2
110instrument aboard the B200 aircraft deployment as part of the first phase of the Department of Energy
111(DOE) Two Column Aerosol Project (TCAP)[21].

112

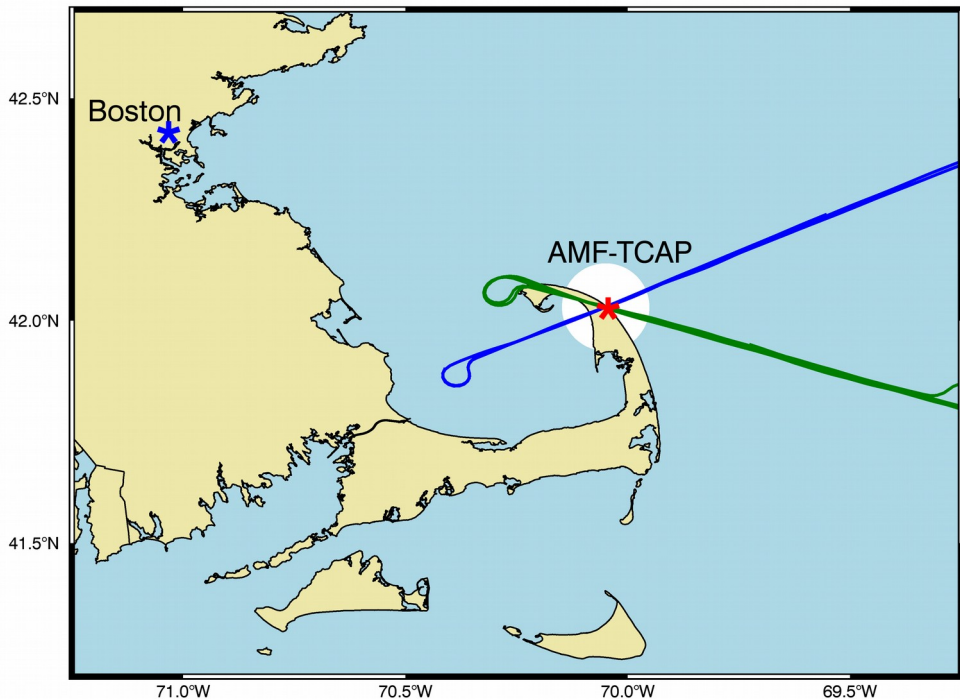
1132. **Methodology**

114

115The first intensive phase of the TCAP field campaign took place in the east coast of North America
116(over Cape Cod, MA, U.S.) through July and part of August 2012. The primary TCAP objectives were
117to characterize the aerosol direct effect under polluted conditions (over Cape Cod, MA), and contrast it
118with pristine conditions several hundred kilometers away from land over the Atlantic Ocean. Here we
119use data collected at the DOE Atmosphere Radiation Measurement (ARM) Mobile Facility (AMF) site
120with the 2-D-MAX-DOAS located at the Highlands Center in the Cape Cod National Seashore about
12185 km southeast of Boston, MA and aboard the NASA B-200 King Air aircraft with the second
122generation HSRL-2 (Fig. 1). Details about the comprehensive set of measurements aboard aircrafts and
123with DOE Atmospheric Radiation Measurement (ARM) Mobile Facility located at the base of the Cape
124Cod are described in Berg et al. [²¹]. We present results for two distinctive cloud-free days with very
125different AOD conditions and when the King Air aircraft carried out overpasses above the TCAP
126ground site (Tuesday 17 July and Sunday 22 July 2012). Fig. 1 shows the NASA's King Air flight
127tracks on both days.

128

129



130

131Figure 1: Map of the Cape Cod Bay area. The TCAP ground-based site is shown with the red asterisk.

132The major city of Boston is shown with the blue asterisk. The NASA's King Air flight tracks on 17 and

13322 July 2012 are indicated with the green and blue lines respectively. The white circle area represents

134the 10 km radius that is used to average the extinction profiles from the HSRL-2.

135

136 **2.1 The 2-D-MAX-DOAS instrument and O₄ retrieval**

137

138The 2-D-MAX-DOAS instrument, including the retrieval of range-resolved NO₂ (3-D distributions),

139are described in detail in Ortega et al. [22]. Briefly, the 2-D-MAX-DOAS instrument as deployed during

140TCAP consisted of three synchronized spectrograph/detector units located indoors in a

141temperature-controlled sea container and the control measurement laptop; the 2-D telescope was

142mounted outdoors on the railing of the seatainer (~45 m ASL), providing an unobstructed view close to

143the horizon towards 0 and 180° azimuth angles (AA) relative to north. The 2-D measurements during

144TCAP provide a unique data set to test and validate diurnal spatial distribution of AOD and aerosol

145microphysical properties, which are part of a separate study. In this work, we use off-axis scans that

146consisted of seven elevation angles (EA) (1, 3, 6, 8, 10, 20, 45° above the horizon, and zenith) and the

147two AAs. The integration time for spectra recorded at each EA was 1 min. The scattered light collected

148with the 2-D telescope was focused into a single CeramOptics 25 m x 1.0 mm silica mono fiber
149coupled to a tri-furcated fiber bundle connected to three Ocean Optics (QE6500) spectrometers with a
150wavelength range between 300 and 631 nm with a spectral resolution between 0.4 - 0.6 nm (FWHM).

151

152The spectra collected at each EA were analyzed using the DOAS method [23] and the WinDOAS
153software package[24]. Details about the retrieval of O₄ dSCDs in the UV and visible, as well as the
154cross sections that were fitted simultaneously are listed in Table 2. All the high-resolution trace gas
155cross sections were adjusted to the instrumental resolution using the slit functions determined close to
156the fit window by means of mercury emission lines. The zenith sky spectra recorded at the start of each
157EA scan is used as reference spectrum to evaluate the O₄ dSCDs from the other EAs. A Ring cross
158section is calculated from the respective reference spectrum using the DOASIS software[31] and
159included in the fit to account for the "filling in" of Fraunhofer lines due to rotational Raman
160scattering[14,32]. An example spectrum of the DOAS analysis of O₄ at 360 and 477 nm is shown in Fig.
1612. We refer to the O₄ dSCDs retrieved over the spectral ranges 338-370 nm and 438-488 nm as the O₄
162dSCDs at 360 and 477 nm, respectively, using the wavelength of the maximum peak absorptions in the
163UV and visible respectively (see Table 2).. We estimate upper limit O₄ dSCD errors of about 7 %
164(~1.80x10⁴² molec²/cm⁵) for 360 nm and 4 % (~1.45x10⁴² molec²/cm⁵) for 477 nm. These errors are
165estimated as the overall variation in O₄ dSCD from sensitivity tests that used different O₄ cross
166sections[2,33], wavelength windows, and polynomial order according with past studies [5,9]. In general,
167the O₄ dSCD variations are about 8 times the DOAS fit error calculated internally in WinDOAS as the
168standard deviations on the retrieved dSCD [24].

169

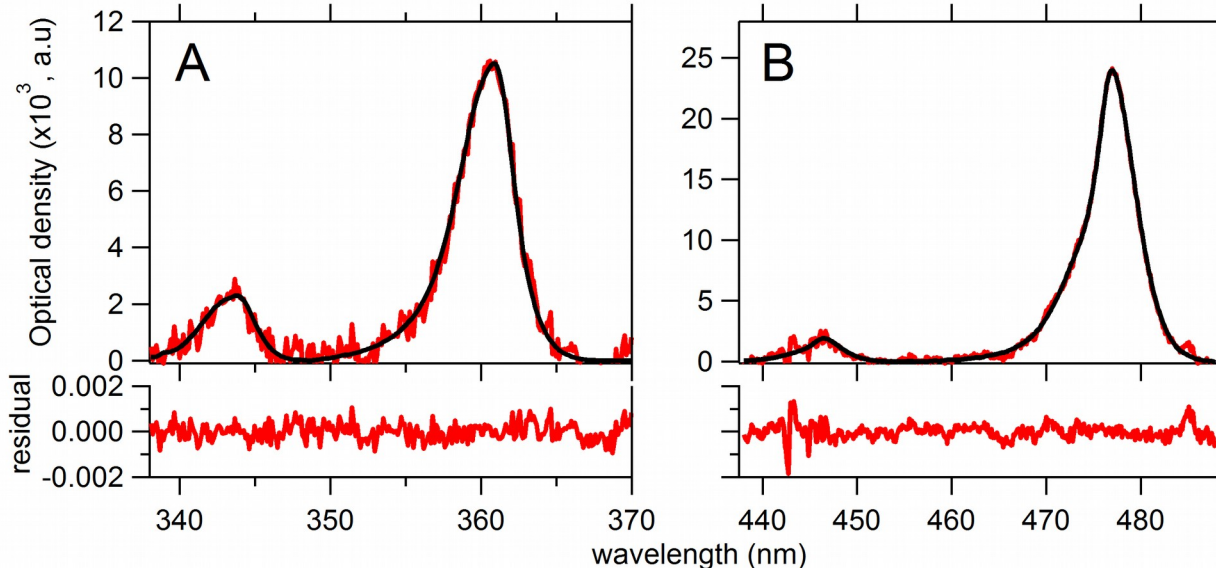
170Table 2: Summary of the DOAS fitting analysis of O₄ in the UV and visible.

Cross section	Fitting window		Reference
	O ₄ (UV)	O ₄ (visible)	
	338 – 370 nm	438 – 488 nm	
O ₄ (293 K)	X	X	Thalman and Volkamer [2]
O ₃ (223 K)	X		Bogumil et al. [25]
O ₃ (243 K)	X	X	Bogumil et al. [25]
NO ₂ (294 K)	X	X	Vandaele et al. [26]
H ₂ O HITEMP (294)		X	Rothman et al. [27]
CHOCHO		X	Volkamer et al. [28]

HCHO	X	Meller and Moortgat. [²⁹]
BrO	X	Fleischmann et al. [³⁰]
Ring	X	Kraus [³¹]
Additional information		
Polynomial	5	5
Intensity offset	Linear (2 terms)	
RTM wavelength (nm)	360	477

171

172



173

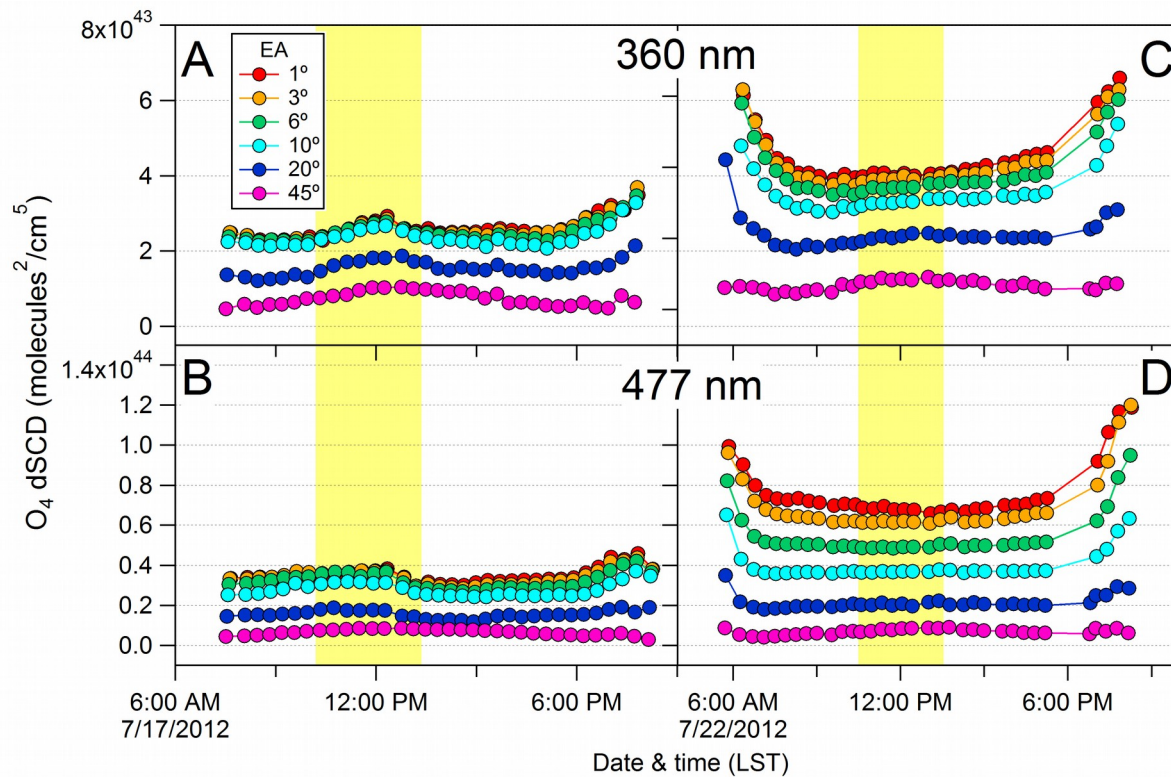
Figure 2: Example of the O₄ fit in the UV and visible using the DOAS settings listed in Table 1. The example is from 17 July 2012 close in time to the NASA's King air overpass (about 11 LST, SZA = 32, EA = 3, and north AA). (A) O₄ analysis in the UV (360 nm). The RMS is 3.93x10⁻⁴ and the O₄ dSCD is 1772.49x10⁴³ molecules²·cm⁻⁵. (B) O₄ analysis in the UV (477 nm). The RMS is 3.29x10⁻⁴ and the O₄ dSCD is 3.65x10⁴³ molecules²·cm⁻⁵. The red lines represent measured spectra and black lines are scaled reference cross sections.

180

The time series of O₄ dSCDs is shown for two cloud-free days, i.e., 17 and 22 July 2012, in Fig. 3. The top panels A and C show the dSCDs at 360 nm, and the bottom panels B and D show the dSCDs at 477 nm. The magnitude and EA dependence of the measured O₄ dSCDs on both days are quite different and serve to inform qualitatively on atmospheric and AOD conditions. On 17 July the small O₄ dSCDs in the low EAs indicate high AOD. For comparison, the clear splitting and higher O₄ dSCDs along the

186 different EAs on 22 July indicate lower AOD. In general, the instrument horizontal distance sensitivity
 187 is enhanced for low AOD. The aerosol extinction profiles and the AOD are examined in Section 2.2.
 188 The yellow shaded areas in Fig. 3 represent the periods of time when two overpasses were carried out
 189 with the NASA King Air above the TCAP ground site and that were used to simulate and compare the
 190 O_4 dSCDs.

191



192

193 Figure 3: Time series of the O_4 dSCDs obtained with the elevation angle scan on 17 July (A and B) and
 194 22 July 2012 (C and D). The north AA is shown. The 360 and 477 nm are shown on top and bottom
 195 respectively. The yellow shaded areas characterize the period of time used to simulate and compare the
 196 O_4 dSCDs and where the NASA's King air carried out overpasses above the TCAP ground site.

197

198 2.2 The High Spectral Resolution Lidar – 2 (HSRL-2)

199

200 The HSRL-2, an improved version of the airborne HSRL-1 instrument [34], measures profiles of
 201 particle backscatter coefficients and linear particle depolarization ratios at 355, 532, and 1064 nm; and
 202 particle volume extinction coefficients at 355 and 532 nm [35]. During TCAP, data were sampled at 100
 203 m horizontal and 15 m vertical resolutions using the nadir-viewing geometry below the aircraft. The
 204 aircraft altitude was about 8 km above ground level during all flights. Hair et al. [34] describes the

205determination of 532 nm aerosol extinction coefficient from the measured power in the molecular
206channel. The molecular extinction is calculated from modeled density profiles. The calculation of
207aerosol extinction is only performed where the overlap function is unity (approximately 2.5 km from
208the aircraft). The 355 nm aerosol extinction is computed in a similar manner. To avoid ground return
209issues, the extinction profiles start at about 165 m above the surface. Below this altitude we assume
210homogeneous mixing of aerosols and use a constant extinction values measured at 165 m. For detailed
211information about the HSRL-2 instrument and the TCAP deployment, see Muller et al. [36]. Fig. 1
212shows the NASA's King Air flight tracks close to the ground site on the two selected days.

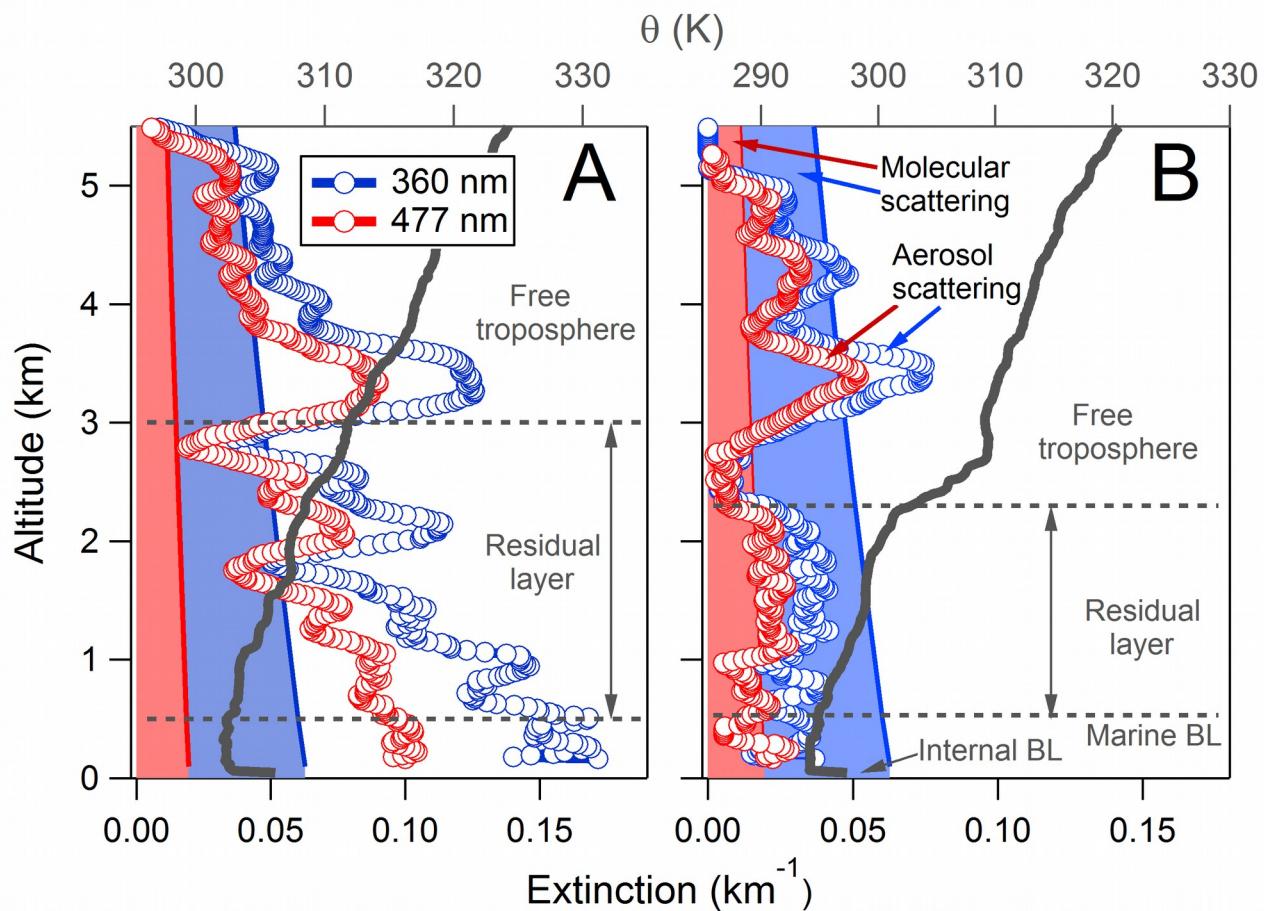
213

214Fig. S1 in the supporting information shows the curtain aerosol extinction profiles at 532 nm obtained
215on both days during the entire flight time, highlighting the overpasses above the ground site. We have
216averaged the HSRL-2 extinction profiles for segments when the aircraft was within 10 km radius of the
2172-D-MAX-DOAS location (white circle of Fig. 1). The 10 km radius used to average the HSRL-2
218captures well the horizontal path length realized by the 2-D-MAX-DOAS, especially on 17 July when
219the path length calculated from the O₄ dSCDs and O₄ concentration ranges from ~ 9 km (360 nm) to 13
220km (477 nm) for an EA of 6° [22]. On 22 July, the horizontal path length was greater due to smaller
221AOD, and ranged from 13 km (360 nm) to 19 km (477 nm) for an EA of 6°. However, the HSRL-2
222aerosol extinction profile averaged over a radius of 20 km is very similar to that obtained with the 10
223km radius.. The difference in MAX-DOAS O₄ dSCDs obtained using the HSRL-2 aerosol extinction
224profile averaged over a radius of 20 km and over a radius of 10 km is about 0.1%. On 17 July the flight
225track was from southeast to northwest, returning by following a similar flight track after ~1.5 hours.
226The first and second overpass time averages are at 11:35 and 13:00 LST. On 22 July the flight track
227was similar but from northeast to southwest at 12:12 LST with similar return track at 12:53 LST.

228

229The averaged extinction profiles at 360 and 477 nm, where O₄ has strong absorption bands, were
230calculated using the extinction Angstrom exponent between the standard wavelengths of 355 and 532
231nm. As an example, Fig. 4 shows the averaged aerosol extinction profiles at 360 and 477 nm obtained
232during the second overpass on both days. On 17 July, the aerosol extinction was significantly higher
233than on 22 July as previously identified with the O₄ dSCDs. The inhomogeneity of AOD around the
234ground site was assessed by calculating the AOD below the aircraft altitude down to the surface from
235the profiles as observed when the airplane was on the west and east sides above the 2-D-MAX-DOAS
236measurement site within the same overpass (see Fig. 1). The average AOD at 477 nm during the first
237overpass (11:35 LST) on 17 July was 0.253 with a variability of 0.001 calculated as the difference

238 between the AODs integrated from HSRL-2 extinction profiles measured towards the east and west of
 239 2392-D-MAX-DOAS site. The average AOD during the second overpass (13:00 LST) was 0.313 with a
 240 slightly higher variability of 0.045 between the east and west directions. On 22 July, the average AOD
 241 was 0.093 (± 0.005) for the first overpass (12:12 LST) and 0.108 (± 0.001) for the second overpass
 242 (12:53 LST). As can be seen, for most of the time homogeneity within 2 % percent was identified,
 243 except on the second overpass on 17 July where AOD varied by about 10%. The molecular scattering
 244 using the method reported by Bodhaine et al. [37] is calculated at 360 and 477 nm to compare with the
 245 extinction profile as measured by the HSRL-2 (see Fig. 4). As can be seen on 17 July, the extinction
 246 due to the aerosols was consistently higher below 2 km. On the other hand, on 22 July the aerosol
 247 extinction below 2 km is very close to or even lower (especially for the 360 nm) than the molecular
 248 scattering.



249
 250 Figure 4: Averaged HSRL-2 aerosol extinction profiles obtained during the overpasses on (A) 17 July
 251 2012, and (B) 22 July 2012 (< 10 km radius). The filled area indicates extinction due to molecular
 252 scattering. The potential temperature (θ) profiles derived from radiosondes launched at the AMF site

253are shown in continuous gray lines. The dotted horizontal lines indicate the approximate altitude of the
254marine BL, residual layer, and free troposphere.

255

256Elevated aerosol layers were frequently observed during TCAP[²¹]. The potential temperature profile
257for both case study days is shown in Fig. 4 and reveals a relatively shallow marine BL (~400 m), an
258internal BL associated with warming of the Cape Cod peninsula (0 – 60 m), a decoupled residual layer
259above the mixed layer, and elevated aerosol layers in the free troposphere. For a detailed
260characterization of these elevated aerosol layers see Berg et al. [²¹]. Here, we use the potential
261temperature profiles to calculate partial AOD columns in the BL, residual layer, and in the free
262troposphere. The partial AOD contained in the free troposphere represented 32 % (360 nm) and 36 %
263(477 nm) on the first overpass and 35 % (360 nm) and 36 % (477 nm) during the second overpass on
26417 July. On 22 July the partial AOD above 2 km were even higher: 51 % (360 nm) and 56 % (477 nm)
265for the first overpass and 56 % (360 nm) and 61 % (477 nm) for the second overpass.

266

267 2.3 Additional measurements

268

269The additional suite of measurements used to complement our study are the atmospheric temperature
270and pressure profiles provided by the radiosondes, which were launched four times a day at the AMF
271site (~ 00, 05, 17, and 23 UTC). The vertical resolution of the sondes was about 10 m reaching a
272maximum altitude of about 28 km. For this study, the closest radiosonde in time (17 UTC or 13:00
273LST) is used to construct the O₄ concentration profile and to prescribe the temperature, pressure and
274relative humidity in the RTM (see Section 2.4).

275

276Further comparison of the AOD measured by HSRL-2 with ground-based multifilter rotating shadow
277band radiometer (MFRSR)[³⁶], and a Cimel Sun photometer[³⁹] showed good agreement, with AODs
278retrieved by the HSRL-2 generally being 5-10% smaller than the ground-based AOD, indicating that 90
279-95% of the aerosol extinction was indeed located below the aircraft. The small difference could be due
280to underestimation of the aerosols in the very shallow aerosol layer near the surface (< 165 m) where
281the HSRL-2 loses sensitivity (ground return), or due to aerosol extinction in layers located above the
282aircraft altitude of approximately 8 km.

283

284 2.4 Radiative Transfer Modeling

285

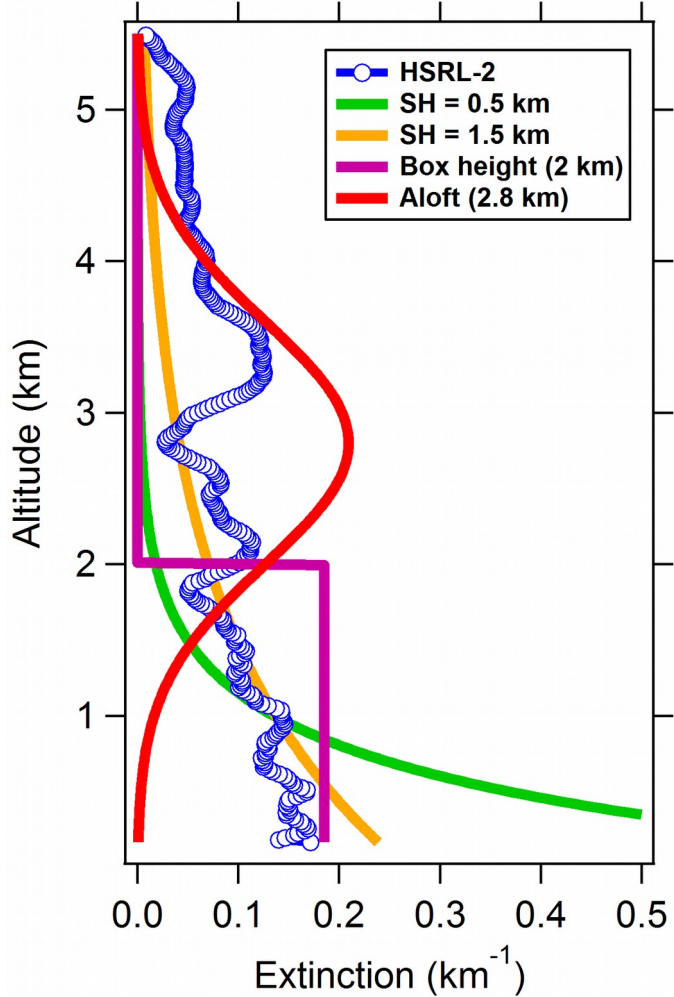
286The simulation of the O₄ dSCDs was performed using the full spherical Monte-Carlo atmospheric
287radiative transfer model (McArtim)[⁴⁰]. McArtim was initialized using the geometry of the EA scan

288performed with the 2-D-MAX-DOAS during TCAP. The altitude grid used in the radiative transfer
289calculations to forward model the O₄ dSCDs was set to 100 m thickness between 0 and 12 km, 1 km
290thickness between 12 and 25 km, and 2.5 km thickness between 25 and 100 km. The average aerosol
291extinction profile in 100 m thickness layers obtained with the HSRL-2 is used between 0 and 8 km to
292represent the air mass probed by the HSRL-2. The wavelengths chosen to forward model the O₄
293dSCDs were 360 and 477 nm. Pressure and temperature profiles up to 28 km were taken from the
294radiosonde (Section 2.3) adjusted to this altitude grid. Above 28 km the U.S standard atmosphere was
295used. When the 2-D-MAX-DOAS was pointing towards the south, the land surface albedo obtained
296from atmospheric transmission by the co-located MFRSR^[41] was used (0.04 at 360 nm, and 0.05 at
297477 nm). When pointing to the north, which mostly sees the ocean; we assumed a Lambertian surface
298albedo of 0.07 for both wavelengths^[42]. Additional aerosol optical parameters consisted of a single
299scattering albedo, ssa, of 0.98^[36], and the aerosol phase function represented by an asymmetry
300parameter, g , of 0.68 (Greenstein approximation), which are typical for this location^[43]. We have
301conducted sensitivity studies that varied ssa (± 0.05) and g (± 0.05) and found a small effect (< 2 %
302total) on the simulation of O₄ dSCDs. Similar findings are presented in Clémer et al. [5] and Baidar et
303al. [8]. For the comparison with the measurements, RTM calculated O₄ SCDs of the zenith view were
304subtracted from SCDs at other elevation angles.

305

306Sensitivity studies were further performed that varied the aerosol extinction profiles while keeping the
307AOD constant (constrained by HSRL-2). Fig. 5 shows the different aerosol extinction profiles created
308to test the sensitivity of simulated O₄ dSCDs. We use two aerosol profiles exponentially decreasing
309with altitude, one with a scale-height (SH) of 0.5 and the other with SH of 1.5 km (orange and green
310lines in Fig. 5); a homogeneous aerosol extinction profile with a height of 2 km was assumed to
311represent well-mixed homogeneous BL; and the red profile in Fig. 5 represents the extinction profile
312assumed to be aloft with a Gaussian shape. The maximum extinction of this profile is at 2.8 km and a
313width of 0.8 km. To compare with the real extinction profiles we also use the profiles retrieved with the
314HSRL-2 interpolated to the RTM grid vertical resolution.

315



316

317Figure 5: Example of aerosol extinction profile shapes assumed at 360 nm to constrain the RTM. All
 318the extinction profiles are constrained by the AOD obtained with the HSRL-2, i.e., all have the same
 319AOD. In this example we used the extinction profile at 360 nm obtained on 17 July.

320

3213. Results and discussions

322

323The sensitivity studies presented in Section 3.1 have in common that the AOD was constrained to that
 324measured by HSRL-2, and the aerosol extinction profile shape was varied. In Section 3.2 we present
 325additional sensitivity studies to further assess the influence of the elevated aerosol layers. In this case,
 326the HSRL-2 aerosol extinction below 2 km was used, while the aerosol extinction above 2 km was set
 327to zero. The following sections discuss TCAP results in context with the available literature about
 328elevated aerosol layers (Section 3.3), CF_{O_4} found with previous MAX-DOAS measurements (Section
 3293.4). Finally, Section 3.5 summarizes the need for future research and gives an Outlook.

330

3313.1 Comparison of measured and simulated O₄ dSCDs

332

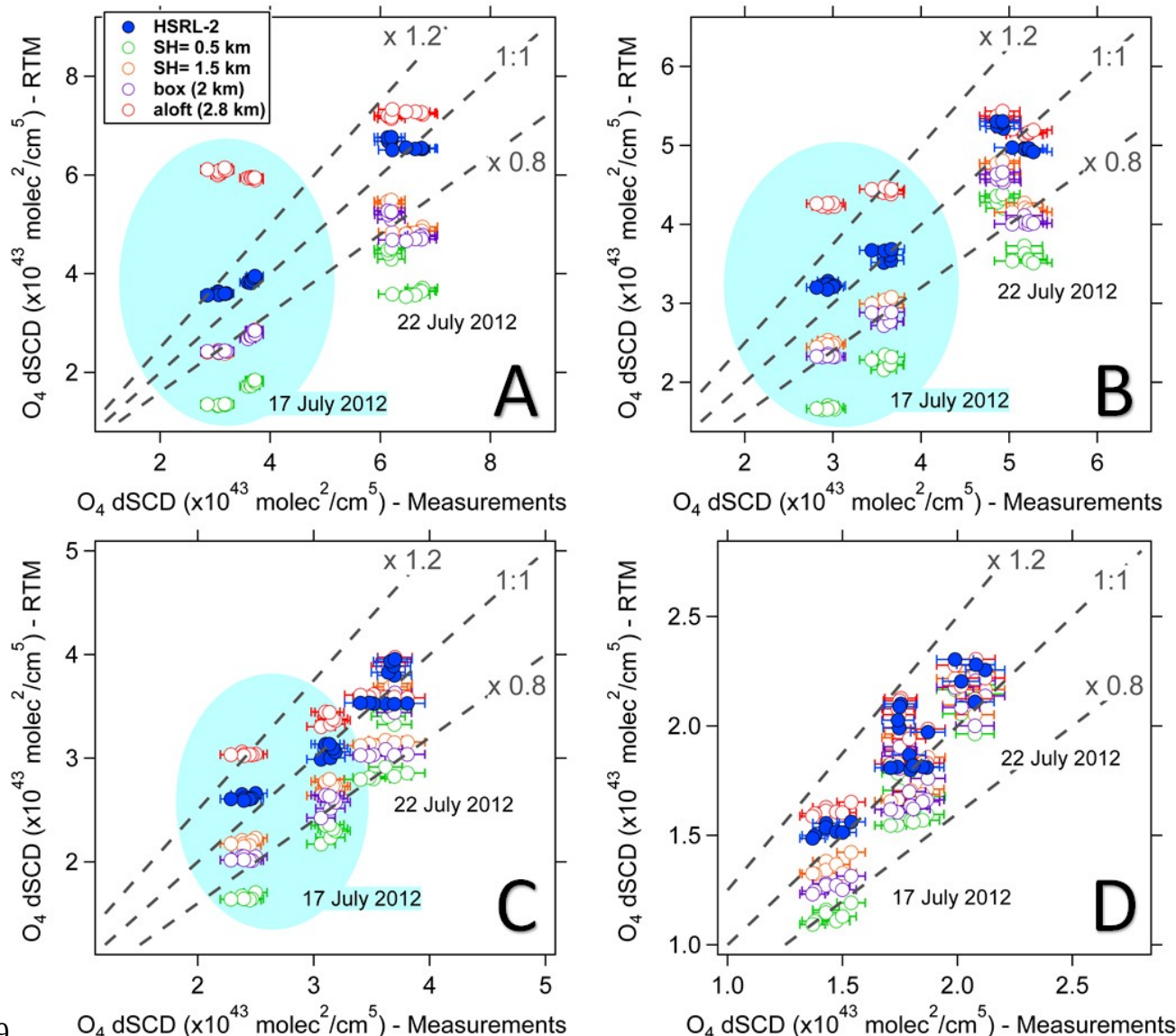
333Fig. 6 shows the comparison of simulated and measured O₄ dSCDs for different EAs (3°-A; 6°-B; 33410°-C; and 20°-D) at 477 nm. The data shown here represent both AAs, and both days. The four EAs 335were chosen to represent a range of low and high angles that are sensitive to the air masses probed by 336the HSRL-2. The different aerosol scenarios used during simulations are represented using the same 337color scheme as that of Fig. 5. Note that for clarity the axis scale is different for each EA. The light blue 338shaded area for the low EAs ($\leq 10^\circ$) shows the values obtained on 17 July – high AOD. This clear split 339in the O₄ dSCDs is caused by the significant differences in the aerosol extinction magnitude on both 340days. However, the magnitude of the O₄ dSCDs for the EA of 20° (D) is less influenced by changes in 341AOD and profile shapes. A similar effect was also observed by Clémer et al. [5]. They identified that 342high elevation angles ($> 15^\circ$) are rather insensitive to small AOD changes (< 0.15 , 360 nm) when using 343exponentially decreasing profiles with SH from 0.25 to 0.75 km. It is apparent from this figure that the 344simulated O₄ dSCDs assuming aerosol extinction located in the BL are consistently lower than the 345measurements. The correlation under such conditions is always below the 1:1 line, or even below the 346x0.8 line. In particular, the exponential decrease with a SH = 0.5 km shows the largest differences. On 347the other hand, the O₄ dSCDs are overestimated if the aerosol extinction is assumed to be only aloft 348(red circles), in particular in the low EAs. The comparison improves significantly and consistently for 349all EAs if the simulations are performed using the extinction profiles retrieved with the HSRL-2 (filled 350blue circles). In this case, the measured O₄ dSCDs are close to the 1:1 line for all EAs. A similar figure 351for 360 nm (with similar findings) can be found in the supporting information (Fig. S2).

352

353 The overall comparison between simulated and modeled O₄ dSCDs at both wavelengths, all EAs, both 354AAs, and both days is shown in Fig. 7. The O₄ dSCDs located in the lower left corner are from 17 July 3552012 (high AOD); higher O₄ dSCDs correspond to low EAs on 22 July 2012 (low AOD, see Sect. 2.2). 356The overall qualitative evaluation confirms that the simulated O₄ dSCDs are underestimated if the 357assumption is made that aerosol extinction is located only in the BL; and the comparison improves if 358the extinction profiles retrieved with the HSRL-2 are used. We have noticed an AA dependency. In 359general, the southerly viewing angle contains smaller O₄ dSCDs that are closer to the 1:1 line if using 360the HSRL-2. On the other hand, the simulated northerly view yields slightly higher simulated O₄ 361dSCDs. This may be explained by the fact that we use average extinction profiles from the HSRL-2, 362and the instantaneous air mass measured by the 2-D-MAX-DOAS may be slightly different. However, 363the 1:1 line is within the error bars with averages of $6.4 \pm 0.4\%$ (360 nm) and $4.7 \pm 0.6\%$ (477 nm) if

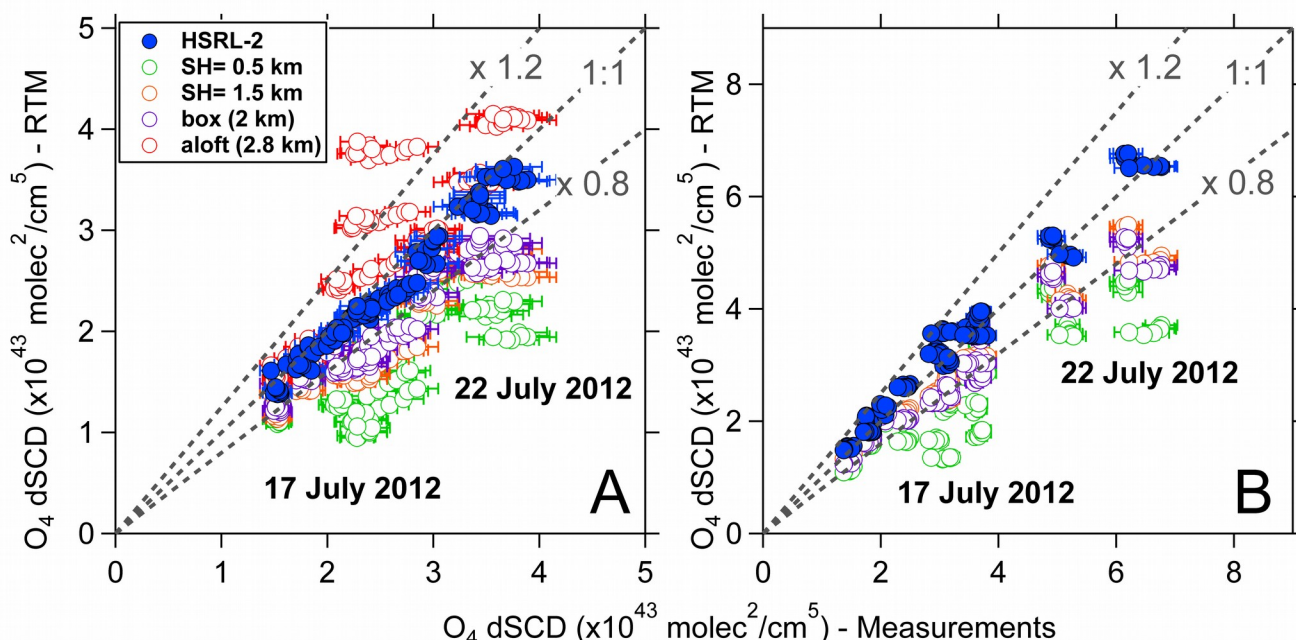
364 using the HSRL-2 measurements. For aerosol homogeneous conditions in the marine BL, Volkamer et
 365 al. [9] showed that comparison of measured and simulated O_4 SCD agreed within $1 \pm 2\%$ in the lower
 366 400 m close to the surface when the aerosol extinction aloft is characterized by independent
 367 measurements under similar air masses.

368



369
 370 Figure 6: Comparison of O_4 dSCDs measured and simulated at 477 nm for the elevation angles of (A)
 371 13° , (B) 6° , (C) 10° , and (D) 20° . Note that the x-axis scales are different for each elevation angle. The
 372 light blue shaded oval represents values from 17 July, which are easily identified for low elevation
 373 angles ($\leq 10^\circ$). For the elevation angle of 20° there is not an apparent split in the O_4 dSCDs for the
 374 different days (the light blue shaded oval is not shown). The O_4 dSCD error bars in the measurements
 375 represent the 4% described in Section 2.1.

377A linear regression analysis was used to assess the effect of aerosol extinction profiles quantitatively for
 378the different EAs. The different sets of simulated O_4 dSCDs were compared to the measurements with a
 379two folded goal: (1) to identify a typical bias with the assumed extinction profiles and (2) to create a
 380proxy for the CF_{O_4} based on statistical analysis. To achieve the first goal the linear regression was
 381calculated in the form $y = mx + b$ where y is the simulated and x is the measured O_4 dSCDs; m is the
 382slope and b the intercept in $molec^2/cm^5$. The results of the linear correlation analysis using this
 383approach are presented in Table 3. This Table shows the results among different EAs, for all EAs, and
 384for the two wavelengths. Interestingly, the slope increases as the EA increases in all cases when the
 385aerosol is assumed to be in the BL. This behavior is observed consistently at both wavelengths. In
 386general, the offset (bias) is negative and higher than the O_4 dSCD error. These results suggest that the
 387low EAs are highly sensitive towards aerosol layers aloft. This particular pattern is not observed if
 388either the extinction profiles of the HSRL-2 or the aerosol assumed extinction aloft is used to initialize
 389the RTM. Table 4 also shows the overall slopes and intercepts if data from all EAs are fitted
 390simultaneously. Interestingly, the slope is smaller than unity when assuming aerosol extinction profiles
 391in the BL. The overall correlation coefficients (R^2) improve significantly (0.98) by using the HSRL-2
 392extinction profiles with a slope close to unity. In general, the correlations decrease by assuming the
 393extinction to be in the lower part of the atmosphere. This general approach to evaluate slopes and
 394intercepts may potentially help future studies to better constrain elevated aerosol layers.



397Figure 7: Comparison of O_4 dSCDs measured and simulated at (A) 360 nm and (B) 477 nm. The
 398correlation plot includes all the EAs with the extinction profiles shapes assumed and measured (Fig. 4.)
 399

400Table 3: Results from the linear correlation analysis of the simulated and measured O_4 dSCDs using the
 401EAs of 3° , 6° , 10° , 20° and the aerosol extinction profiles from Fig. 3. The analysis is performed using
 402the linear model $y = mx + b$, where m is the slope and b the intercept.

Profile shape	EA ($^\circ$)	Slope (360/477 nm)	Intercept $\times 10^{43} \text{ molec}^2 \cdot \text{cm}^{-5}$ (360/477)	R^2 (360/477 nm)
Exp decrease (SH = 0.5 km)	3	$0.77 \pm 0.05 / 0.78 \pm 0.06$	$-0.76 \pm 0.15 / -1.02 \pm 0.27$	0.92/0.90
	6	$1.10 \pm 0.07 / 1.03 \pm 0.08$	$-1.34 \pm 0.20 / -1.35 \pm 0.34$	0.92/0.88
	10	$1.27 \pm 0.07 / 1.19 \pm 0.09$	$-1.42 \pm 0.18 / -1.28 \pm 0.28$	0.93/0.89
	20	$1.26 \pm 0.10 / 1.48 \pm 0.12$	$-0.73 \pm 0.18 / -0.98 \pm 0.20$	0.86/0.88
	3, 6, 10, 20	$0.53 \pm 0.05 / 0.59 \pm 0.04$	$0.34 \pm 0.13 / 0.37 \pm 0.14$	0.53/0.73
Exp decrease (SH = 1.5 km)	3	$0.80 \pm 0.04 / 0.81 \pm 0.04$	$-0.34 \pm 0.12 / -0.09 \pm 0.22$	0.95/0.94
	6	$0.95 \pm 0.05 / 0.90 \pm 0.06$	$-0.56 \pm 0.16 / -0.17 \pm 0.27$	0.93/0.90
	10	$1.00 \pm 0.06 / 0.97 \pm 0.07$	$-0.57 \pm 0.15 / -0.20 \pm 0.23$	0.93/0.90
	20	$1.03 \pm 0.09 / 1.22 \pm 0.11$	$-0.34 \pm 0.17 / -0.39 \pm 0.20$	0.83/0.83
	3, 6, 10, 20	$0.70 \pm 0.03 / 0.75 \pm 0.02$	$0.14 \pm 0.07 / 0.39 \pm 0.08$	0.88/0.93
Box (2 km)	3	$0.79 \pm 0.03 / 0.75 \pm 0.04$	$-0.14 \pm 0.11 / 0.10 \pm 0.20$	0.95/0.94
	6	$0.93 \pm 0.05 / 0.90 \pm 0.07$	$-0.46 \pm 0.14 / -0.33 \pm 0.28$	0.94/0.89
	10	$1.05 \pm 0.06 / 1.02 \pm 0.08$	$-0.61 \pm 0.15 / -0.47 \pm 0.25$	0.93/0.89
	20	$1.10 \pm 0.09 / 1.30 \pm 0.11$	$-0.38 \pm 0.17 / -0.60 \pm 0.19$	0.85/0.87
	3, 6, 10, 20	$0.71 \pm 0.02 / 0.73 \pm 0.02$	$0.22 \pm 0.06 / 0.34 \pm 0.07$	0.90/0.94
Aloft (2.8 km)	3	$0.24 \pm 0.02 / 0.38 \pm 0.02$	$3.21 \pm 0.05 / 4.76 \pm 0.11$	0.90/0.94
	6	$0.39 \pm 0.02 / 0.48 \pm 0.03$	$2.17 \pm 0.06 / 2.81 \pm 0.13$	0.94/0.92
	10	$0.52 \pm 0.03 / 0.57 \pm 0.05$	$1.35 \pm 0.09 / 1.65 \pm 0.14$	0.92/0.88
	20	$0.73 \pm 0.09 / 0.92 \pm 0.11$	$0.45 \pm 0.16 / 0.31 \pm 0.19$	0.74/0.77
	3, 6, 10, 20	$1.01 \pm 0.07 / 1.05 \pm 0.06$	$0.30 \pm 0.18 / 0.57 \pm 0.22$	0.69/0.77
HSRL-2	3	$1.00 \pm 0.04 / 0.92 \pm 0.03$	$-0.16 \pm 0.12 / 0.66 \pm 0.12$	0.97/0.97
	6	$0.96 \pm 0.04 / 0.88 \pm 0.05$	$-0.06 \pm 0.12 / 0.58 \pm 0.21$	0.96/0.93
	10	$0.94 \pm 0.04 / 0.87 \pm 0.06$	$-0.01 \pm 0.12 / 0.48 \pm 0.19$	0.95/0.91
	20	$0.89 \pm 0.09 / 1.07 \pm 0.11$	$0.10 \pm 0.16 / -0.01 \pm 0.19$	0.81/0.82
	3, 6, 10, 20	$0.94 \pm 0.01 / 0.99 \pm 0.02$	$0.01 \pm 0.04 / 0.18 \pm 0.06$	0.98/0.98

403

404The quantitative estimation of the CF_{O_4} was calculated by forcing the intercept to zero, i.e., linear

405model of $y = mx + 0$ where the slope represents the proxy for the CF_{O_4} . Results of this analysis are
 406shown in Table 4. In general, the correlation using all EAs reveal that CF_{O_4} between 0.65 - 0.85 are
 407needed when the assumed extinction is located in the BL. One interesting finding is that for these
 408conditions at lower EA a lower CF_{O_4} is needed. This is contrary to findings by Irie et al. [18] where they
 409show lower CF_{O_4} values at higher EAs and with the empirical form of $1 - EA/60$. However, Irie et al.
 410[18] pointed out that uplifted aerosol layers were not observed using ground-based Lidar. Interestingly,
 411they found good agreement between near-surface extinction values with independent measurements
 412without correction factor, although higher residuals at high EAs ($> 20^\circ$). This is consistent with the way
 413that aerosol layers above significantly impact the O_4 dSCDs measured with low EAs. This strong EA
 414dependency in the CF_{O_4} is not found if the RTM is constrained by the HSRL-2 extinction profiles.

415

416Our results indicate that knowledge about the extinction profiles in the BL and aloft are important in
 417order to draw conclusions about the simulation of O_4 dSCDs. Assuming the aerosol extinction to be
 418purely in the BL in combination with the application of the CF_{O_4} would yield good agreement with
 419independent co-located AOD observation. However, the real aerosol extinction profiles would be
 420different. On the other hand, if the CF_{O_4} is not applied the AOD would be underestimated by up to 60 %
 421(depending on the CF_{O_4} , i.e., depending on the aerosol profile shape). Furthermore, if the goal is to
 422retrieve aerosol extinction in the near-surface layer using “corrected” O_4 dSCDs this would yield an
 423overestimation of the aerosol extinction coefficients created by the misplacement of aerosols. In fact,
 424Zieger et al. [17] compared the near-surface aerosol extinction coefficients retrieved by MAX-DOAS
 425with in-situ measurements and found systematically higher MAX-DOAS values. As mentioned in that
 426study, the presence of aerosols at higher altitudes might result in an overestimation of the lowest
 427extinction values. This is also clear in the assumed extinction profiles from Fig. 5 where all the
 428assumed extinction profiles have the same AOD but higher aerosol extinction coefficients close to the
 429surface, in particular using the exponentially decreasing profiles. These findings are in agreement with
 430independent airborne MAX-DOAS observations, where it has been shown that agreement between
 431measured and simulated O_4 SCD is within $1 \pm 2\%$ error in the BL when aerosols aloft are well
 432characterized independently [9].

433

434Table 4: Same as Table 3 but forcing the intercept to zero, i.e., linear model of $y = mx + 0$.

Profile shape	EA ($^\circ$)	Slope (CF_{O_4})		R^2
		(360/477 nm)	(360/477 nm)	
Exp decrease	3	0.54 ± 0.01	0.58 ± 0.02	0.45/0.51

	6	0.65±0.020/0.72±0.02	0.33/0.43
(SH = 0.5 km)	10	0.74±0.02/0.80±0.02	0.32/0.40
	20	0.85±0.11/0.92±0.02	0.39/0.35
	3, 6, 10, 20	0.65±0.01/0.68±0.02	0.80/0.97
	3	0.70±0.01/0.80±0.01	0.71/0.90
Exp decrease	6	0.76±0.01/0.86±0.01	0.60/0.82
(SH = 1.5 km)	10	0.80±0.01/0.91±0.01	0.58/0.79
	20	0.84±0.01/1.00±0.02	0.55/0.56
	3, 6, 10, 20	0.75±0.01/0.85±0.01	1.02/1.19
	3	0.74±0.01/0.77±0.01	0.85/0.99
Box	6	0.78±0.01/0.83±0.02	0.67/0.74
(2 km)	10	0.82±0.01/0.87±0.01	0.57/0.65
	20	0.89±0.01/0.97±0.02	0.55/0.48
	3, 6, 10, 20	0.78±0.01/0.82±0.01	1.11/1.17
	3	1.24±0.04/1.29±0.06	24.80/11.16
Aloft (2.8 km)	6	1.10±0.04/1.13±0.03	7.75/5.25
	10	1.02±0.03/1.08±0.02	3.58/3.17
	20	0.98±0.01/1.09±0.01	1.35/1.09
	3, 6, 10, 20	1.12±0.02/1.05±0.01	0.85/1.06
	3	0.95±0.01/1.05±0.01	0.97/1.25
HSRL-2	6	0.94±0.01/1.02±0.01	0.93/1.24
	10	0.93±0.01/1.02±0.01	0.91/1.24
	20	0.95±0.01/1.07±0.01	0.92/0.81
	3, 6, 10, 20	0.94±0.01/1.04±0.01	0.92/1.06

435

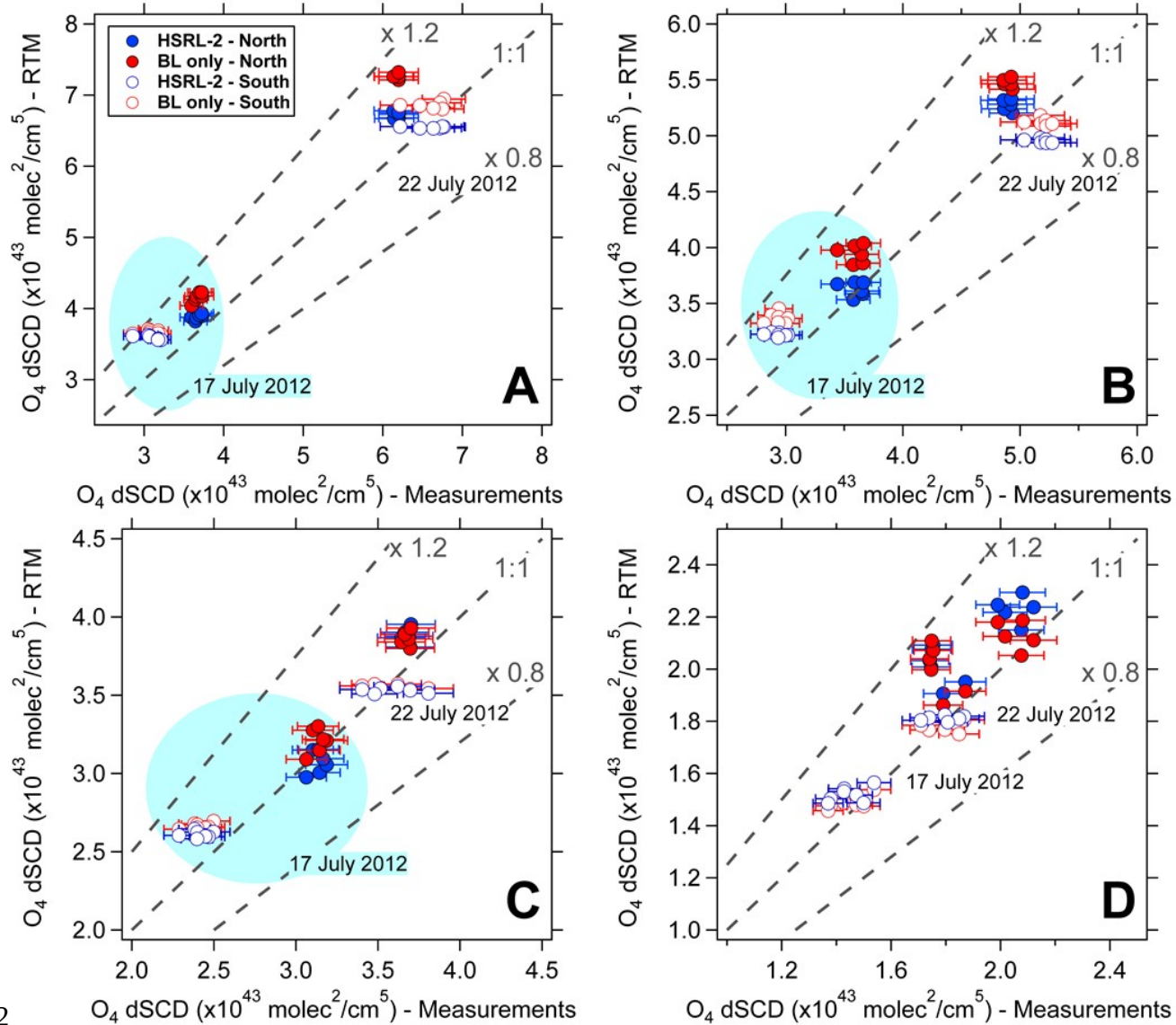
4363.2 Effect of elevated aerosol layers on O₄ dSCDs

437

438Figure 8 shows the comparison of O₄ dSCDs (measured and simulated at 477 nm) for EAs of (A) 3°,
 439(B) 6°, (C) 10°, and (D) 20° using both the HSRL-2 aerosol extinction below 2 km ('BL only', red
 440circles) and the aerosol extinction up to ~ 7 km ('HSRL-2', blue circles). Filled circles represent the
 441north and open circles the south AA. It is interesting to note that the lowest EAs (3° and 6°) show
 442among the largest systematic differences. The predicted O₄ dSCDs are systematically higher when
 443aerosols aloft are ignored. Virtually no effect of the elevated aerosol layers is only observed at EA of
 44410°. At EAs of 20° the elevated layers have the reverse effect compared to the low EAs, i.e., predicted
 445O₄ dSCDs are either unchanged, or systematically lower when aerosols aloft are ignored. This is

446 consistent with the primary effect of elevated aerosol layers being visible in the lower EAs, as shown
 447 by the linear correlation analysis in Section 3.1. An AA dependency is also captured in Fig. 8, which is
 448 shown as time series in Figure S3 in the supplement. The comparison of the simulations reveals
 449 differences in the lower EAs at different AA, which is not seen in the higher EAs. Significantly smaller
 450 differences are observed for the view to the North if elevated layers are accounted for.

451



452

453 Figure 8: Comparison of O_4 dSCDs measured and simulated at 477 nm for the EAs of (A) 3°, (B) 6°,
 454 (C) 10°, and (D) 20°. Red circles are assuming only HSRL-2 aerosol extinction below 2 and blue
 455 circles HSRL-2 aerosol extinction up to ~7 km. The north AA are solids while open circles represent
 456 the south AA.

457

458 The results of the linear regression analysis between the simulated ('BL only') and measured O₄
 459 dSCDs are presented in Table 5. The EA analysis is performed using the approach presented in Section
 460 3.1. Columns 2 to 4 show the results of the linear model $y = mx + b$, while column 5 shows the CF_{O₄}
 461 obtained with the statistical model of $y = mx + 0$. In comparison with Tables 3 (HSRL-2 case) the slope
 462 and intercept are not significant different at 360 and 477 nm, indicating maximal sensitivity to aerosols
 463 in the boundary layer. However, the CF_{O₄} is significantly different for the EA of 3° and 6°, especially at
 464 477 nm. In this case, the CF_{O₄} is larger than 5 % when the aerosols aloft are not taken into account.
 465 Overall, these results confirm that ground based observations of O₄ dSCDs are suitable to identify
 466 elevated aerosol layer and that the sensitivity is enhanced in the visible wavelengths.

467

468 Table 5: Results from the linear correlation analysis of the simulated and measured O₄ dSCDs using the
 469 EAs of 3°, 6°, 10°, 20°, aerosol extinction profiles from 'BL only', and north and south AAs. The
 470 analysis is performed using the linear model $y = mx + b$ (columns 2 to 4) and $y = mx + 0$ (column 5).

EA (°)	Slope (360/477 nm)	Intercept x10 ⁴³ molec ² ·cm ⁻⁵ (360/477)	R ² (360/477 nm)	(C _{FO₄} , slope) (360/477 nm)
3	1.02±0.04/1.00±0.04	-0.29±0.12/0.54±0.21	0.97/0.96	0.94±0.01/1.11±0.02
6	1.00±0.04/0.88±0.05	-0.15±0.13/0.81±0.20	0.96/0.94	0.96±0.01/1.07±0.02
10	0.91±0.04/0.84±0.05	0.12±0.11/0.64±0.15	0.95/0.93	0.95±0.01/1.03±0.01
20	0.80±0.09/0.98±0.13	0.23±0.16/0.10±0.20	0.76/0.77	0.94±0.01/1.05±0.01
3, 6, 10, 20	0.90±0.01/1.06±0.01	0.09±0.01/0.10±0.10	0.90/0.94	0.94±0.01/1.06±0.01

471

472

4733.3 Literature context: frequency of occurrence of elevated aerosol layers

474

475The elevated aerosol layers identified in this work are not unique of the two presented case studies.
476Berg et al. [21] examined in more detail the contribution of layers aloft to AOD during TCAP using six
477research flights carried out with HSRL-2. They found that elevated layers (from 2.64 km to the top of
478the HSRL-2 ~ 7 km) represented as much as 40% of the total AOD in the continental column. On the
479other hand, in the maritime column all of the AOD was associated with aerosol below 2.64 km.
480Furthermore, the occurrence of elevated aerosol layers was examined over the TCAP area using four
481years data from the Cloud-Aerosol Lidar and Infrared Pathfinder satellite (CALIPSO). In this long time
482series analysis more than 60 % of the aerosol layer tops observed between 2 and 5 km are associated
483with layers aloft during the month of July. The importance of such layers was also noted by Goldstein
484et al. [44] in the Southeast of the U.S. They infer that much of the secondary organic aerosol must occur
485above the surface layer to explain the AOD in summer months. Recent studies using long time series
486from CALIPSO have shown that elevated layers are more frequent than expected [45-47].

487

488The Intergovernmental Panel on Climate Change (IPCC) Working Group I of the Fifth Assessment
489Report summarizes the climatology of aerosol extinction vertical profiles globally, highlighting the
490importance of aerosol layers above 1 to 2 km [46]. They show that the average latitudinal vertical cross
491sections of the 532 nm aerosol extinction vertical profiles from CALIPSO during 2010 extended up to 4
492km for the longitudinal bands of 20° W to 40° E and 60 to 120° E, especially for northerly latitudes (~ 0
493to 50° N). Winker et al. [45] used six year data set from CALIPSO to characterize the global
4943-dimensional distribution of tropospheric aerosols, and present evidence that elevated aerosol layers
495(including the free troposphere) are important, and may be low-biased in the CALIPSO data. They
496compare HSRL extinction profiles co-located with CALIPSO overpasses in the eastern Caribbean, the
497Southeast US, and the mid-Atlantic region, and show that profiles obtained from CALIPSO are
498significantly lower (by about 0.002 km⁻¹) above 4 km altitude than the HSRL [45].

499

500All past MAX-DOAS studies that applied the CF_{O₄} (see Table 1) were conducted at northerly latitudes
501(between 35.0 to 52.0° N) and easterly longitudinal bands (between 4° to 117° E), where AOD is
502enhanced, and elevated aerosol layers are frequent [45,46]. According with the zonal mean distribution of
503aerosol extinction profiles obtained by Winker et al. [45] about 63% and 90% of the AOD extend
504roughly to about 1.5 and 3.0 km, respectively at north latitudes, i.e., a significant fraction of AOD is
505located above 1.5 km (~ 37% on average). During TCAP as much as 40% of AOD was located above 3

506km. To the best of our knowledge elevated aerosol layers were not accounted for in the a-priori aerosol
507profiles used by previous MAX-DOAS studies that found a need for CF_{O_4} .

508

509 3.4 Factors influencing the CF_{O_4} in MAX-DOAS

510

511In order to investigate the different factors that contribute to the CF_{O_4} , O_4 SCDs were simulated using
512McArtim for four cases that differ in the assumptions about the temperature, pressure and aerosol
513profile. The assumptions for each of the four cases are listed in Table 6. All O_4 SCDs were simulated at
514477 nm using the geometry of the EA scan performed with the 2-D-MAX-DOAS during TCAP. The
515simulations were carried out for conditions on 17 July (high AOD case study) and 22 July (low AOD
516case study), and the results are shown in Figure 9. Cases 1 and 2 represent the atmospheric conditions
517as characterized by the radiosondes, while cases 3 and 4 assume the temperature and pressure profile of
518the U.S standard atmosphere. Figure S4 shows the comparison of the temperature and O_4 concentration
519profiles using the measured and U.S standard atmospheric conditions for 17 July 2012. Below 13 km
520the measured temperature is 10-12 K larger than that of the U.S standard atmosphere. As a
521consequence, the O_4 concentration is 15 – 18% higher at a given altitude in the U.S standard
522atmosphere. Several previous MAX-DOAS studies assumed the U.S standard atmosphere directly
523and/or use ambient local surface conditions to adjust the U.S standard atmosphere profiles to represent
524the O_4 profile in the RTM [^{5,14-19}]. Cases 1 and 3 use the measured HSRL-2 aerosol profile, while cases
5252 and 4 use the same AOD confined to the lower atmosphere (exponential decreasing profile with a SH
526of 0.5 km, see Fig. 5). We can assume case 1 approximates well the measured O_4 dSCDs, because we
527have shown in Section 3.1 that under known aerosol distributions and air density profiles there is no
528need for CF_{O_4} , and O_4 can be predicted with little error (< 0.1 %) if the temperature and pressure
529profiles are known [²]. Figure 9 compares case 2 (red), case 3 (blue), and case 4 (green) relative to case
5301.

531

532Table 6: Atmospheric and aerosol conditions used in four case sensitivity tests to simulate O_4 SCDs.

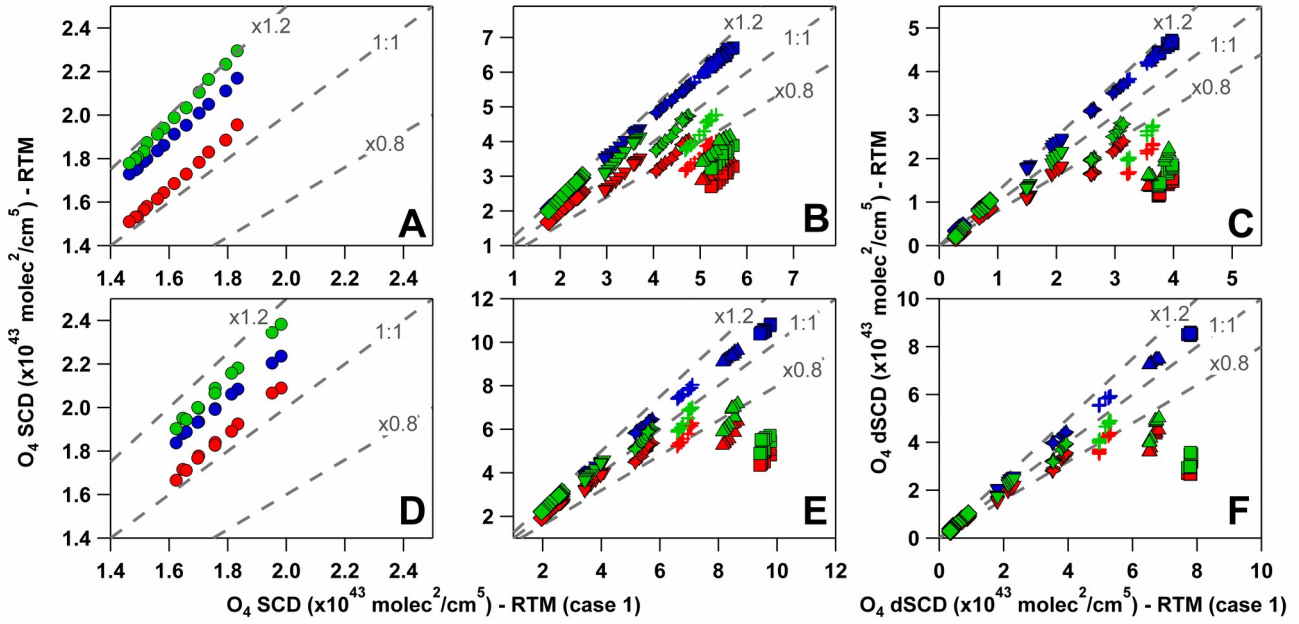
Case #	Atmosphere	Aerosol
1	Radiosonde	HSRL-2
2	Radiosonde	Exponential (SH = 0.5km)
3	U.S atmosphere	HSRL-2
4	U.S atmosphere	Exponential (SH = 0.5km)

533Figure 9 shows three sets of analysis each for the 17 July (AOD ~ 0.35, top row) and 22 July (AOD <

5340.10, bottom row): 1) O_4 SCDs in the zenith view (9A and 9D); 2) O_4 SCDs in the off-axis EAs (9B and 5359E); and 3) O_4 dSCDs using the zenith reference spectrum of the same EA scan sequence. Surprisingly, 536the assumption about the aerosol distribution (case 2) does only have a very minor effect on the O_4 537SCD, which increases by 4 % for both case study days. On the other hand, if the U.S standard 538atmosphere is used (case 3) the O_4 SCDs is overestimated by ~ 18 and 13 % on 17 and 22 July, 539respectively. This corresponds to an O_4 SCD offset (overestimate) of up to 0.1×10^{43} molec 2 cm $^{-5}$. The 540axis scales of Fig. 9B and 9E are different on both case study days due to the difference in AOD. 541Interestingly, while points systematically fall above the 1:1 line in panels A and D (case 2), they fall 542systematically below the 1:1 line in panels B and E, and C and F. Similarly, the O_4 SCDs in the zenith 543view are higher for case 4 than for case 3, but lower for the off-axis angles. We conclude that 544independent of the assumptions about temperature and pressure conditions, a too low distribution of 545aerosols introduces a small but noticeable high bias in the zenith simulated O_4 SCDs, which translates 546in a small low-bias in the O_4 dSCDs for the off-axis EAs. This bias leads to $0.95 < CF_{O_4} < 1$ for all 547cases and EAs. We conclude that the bias of the aerosol profile on the zenith view is small compared to 548the assumptions about vertical distributions of 1) aerosols and 2) air density, which have a major 549influence on the interpretation of the off-axis EAs.

550

551If the aerosol is confined to the BL (case 2) CF_{O_4} is needed at all EAs, especially at high AOD (see 552Table 4). Interestingly, using the U.S standard atmosphere increases the simulated O_4 SCDs for no good 553reason. This leads to a partial compensation of the bias created by the erroneous aerosol profile, and a 554smaller apparent deviation from the 1:1 line for both case study days, and at all EAs (but zenith). The 555assumption about the aerosol being confined in the BL (case 2) yields a negative bias that is 556significantly larger than the bias caused by the assumptions about air density (case 3). Recent studies 557that have used actual measurements of temperature, pressure and humidity profiles in the RTM did not 558find a need for CF_{O_4} [9,19]. If RTM simulations use the U.S standard atmosphere, the bias in the 559predicted O_4 dSCDs depends on the relative difference of the local temperature and pressure conditions 560at the time of measurement to the conditions in the U.S standard atmosphere, which is often not known 561for studies in Table 1. This complicates an assessment of the causes for CF_{O_4} in past MAX-DOAS 562studies. However, it is clear from Figure 9 that the effect of misrepresenting the aerosol profile is 563especially important for $EA < 20^\circ$. Notably, cases 3 and 4 also yield O_4 SCDs above the 1:1 line, but 564only for $EAs \geq 20^\circ$. We conclude that for $EA < 20^\circ$ the negative bias from assuming aerosols to be 565confined to the BL is more important than the assumption about the atmospheric air density profile.



566

567Figure 9: Comparisons of the simulation of O_4 SCDs (A,B,D,E) and O_4 dSCDs (C,F) for case 2 (red),
 568case 3 (blue), and case 4 (green) relative to case 1 (see Table 6) on (top row) 17 July and (bottom row)
 56922 July 2012. Different symbols mark different EAs: (circle) 90, (diamond) 45, (triangle down) 20,
 570(star) 10, (plus) 6, (triangle) 3, and (square) 1 EA.

571

5723.5 Outlook

573

574Ground based MAX-DOAS measurements of O_4 are mostly sensitive to aerosol in the boundary layer.
 575However, the results of this study indicate that such measurements are disturbed in presence of aerosol
 576layers aloft. As a consequence, even O_4 dSCDs measured in the lower EA contain bias due to elevated
 577aerosol layers, which has potential to translate into bias of partial AOD that is attributed to the BL
 578based on O_4 dSCDs alone. Elevated aerosol layers were identified primarily with the visible
 579wavelengths. In order to ovoid bias in the simulation of O_4 dSCDs we recommend the use of actual
 580temperature and pressure vertical profiles in the RTM [9,19,48,49].

581

582Under known atmospheric conditions of temperature and pressure we propose that the pattern of
 583EA-dependent O_4 dSCD offsets can be systematically exploited to help characterize aerosol extinction
 584aloft with ground-based MAX-DOAS, and possibly better characterize these elevated layers. An initial
 585step may be to use total AOD from external sources, e.g., from measurements of the Raman Scattering
 586Probability with the same instrument [50] or independent direct-sun observations (e.g, AERONET) and
 587perform the linear correlation analysis as presented in this work. Friess et al. [4] had developed a

588non-linear inversion based on synthetic spectra and found that O₄ dSCDs are sensitive to aerosol layers
589located about ~3 km altitude. They had suggested that the information content is enhanced when the
590non-linear retrieval inversion uses O₄ dSCDs measured at different wavelengths simultaneously. Our
591results support such sensitivity, which exists at any single O₄ band but mostly at visible wavelengths.
592The simultaneous use of wavelength dependent O₄ dSCD offsets, optimized viewing geometries, and
593external constraints to AOD is promising to maximize information to characterize layers aloft. The
594retrieval of aerosol extinction profiles and partial AODs in the boundary layer and free troposphere,
595especially elevated aerosol layers, deserves further investigation. The TCAP dataset provides a unique
596opportunity to apply, further develop and test state-of-the-art retrievals of elevated aerosol layers. The
597data of the two case studies described here is available for collaborative studies upon request from the
598authors.

599

600Finally, to develop a complete picture about the need for CF_{O4} with ground-based MAX-DOAS, a study
601in the absence of elevated aerosol layers, that has aerosols confined to the BL and benefits from
602collocated independent quantitative measurements of highly vertically resolved and multispectral
603aerosol extinction profiles and atmospheric conditions remains desirable.

604

605**4. Summary and conclusions**

606

607We have presented a detailed study of the simulation of O₄ dSCDs under conditions when the aerosol
608extinction profiles are well-known. We conclude the following:

- 609 • Excellent agreement is found between measurements and simulation of O₄ dSCDs using
610 independently measured, highly vertically-resolved aerosol extinction profiles. A linear
611 correlation has slope close to unity, no significant offset, and R² > 0.98. In particular, no
612 evidence for CF_{O4} is found at 360 and 477 nm, under conditions of high and low AOD.
- 613 • The dominant fraction of the AOD (between 47 to 68 %) was present in form of elevated
614 aerosol layers. Although maximum sensitivity is achieved close to the surface we show that
615 even for low AOD (near molecular scattering dominant conditions), ground-based O₄ dSCD
616 measurements, mainly at 477 nm and low EAs, show sensitivity to such elevated aerosol layers.
617 When elevated aerosol layers are present and total AOD is used in the boundary layer to
618 constrain O₄ simulations a slope that is consistently smaller than unity (0.53 – 0.75), and an
619 offset that is greater than the O₄ dSCD errors of 1.80x10⁴² molec²/cm⁵ for the 360 nm and

620 1.45×10^{42} molec²/cm⁵ for the 477 are found. A proxy for the CF_{O₄} is estimated, and the range of
621 CF_{O₄} is found to be consistent with values that have been reported in recent MAX-DOAS
622 studies.

623 • An EA analysis revealed a consistent and significant negative bias in the O₄ dSCD simulations
624 for all EAs if AOD is high and aerosol distributions are confined to near the surface. The same
625 effect is found when the AOD is small (AOD < 0.1 at 477 nm), however only for EA < 10°. If
626 the EA-dependent bias (intercept in Table 3) is ignored, this manifests as a systematic EA
627 dependence of CF_{O₄} that is most pronounced in the lowest EAs, and equivalent to an
628 overestimation of near-surface extinction.

629 • We propose that the pattern of EA-dependent O₄ dSCD offsets can be systematically exploited
630 in combination with external constraints to AOD to better characterize these elevated layers
631 with ground-based MAX-DOAS.

632 • The aerosol layers aloft identified in this work were not a peculiarity of the two case studies we
633 have selected to investigate, but were frequently observed in a period of four years in the Cape
634 Cod bay area [21]. Future studies might need to consider the impact of such layers on the
635 scattering of sunlight as seen by ground-based passive remote sensing instruments.

636
637 There is now consistent evidence from MAX-DOAS, DS-DOAS and AMAX-DOAS
638 measurements[9,19] that suggests CF_{O₄} are small or not needed if there is enough information about
639 aerosols. A recent study has shown that there is no fundamental limitation on using O₄ dSCDs to
640 constrain aerosol extinction profiles from aircraft[9]. O₄ simulations need to take into account the
641 possibility of elevated aerosol layers. Unless they are accounted for, elevated aerosol layers can result
642 in the overestimation of extinction coefficients near the surface. The retrieval of aerosol profiles by
643 MAX-DOAS is not limited to O₄, and is particularly promising if O₄ is combined with other
644 parameters that constrain AOD, such as the Raman scattering probability[14,50]. The implication of
645 elevated aerosol layers for the interpretation of other trace gases deserves further investigation.

646

647 *Acknowledgements.* The 2-D-MAX-DOAS instrument was developed with support from the
648 NSF-CAREER award ATM-0847793, and US Department of Energy (DoE) award DE-SC0006080
649 supported the TCAP deployment. Ivan Ortega is recipient of a NASA Earth Science graduate
650 fellowship. The authors are grateful to Tim Deutschmann for providing support with the McArtim
651 RTM. The authors thank the entire TCAP team for their support during the campaign. We further thank

652Rick Wagener and Laurie Gregory for providing the AERONET data, Gary Hodges and Kathy Lantz
653for providing the NOAA MFRSR data, and Caroline Fayt and Michel van Roozendael for providing the
654WinDOAS software, and Thomas Wagner for helpful discussions.

655

656**Reference List**

657

658[1] G. D. Greenblatt, J. J. Orlando, J. B. Burkholder, A. R. Ravishankara, Absorption measurements of
659oxygen between 330 and 1140 nm, *Journal of Geophysical Research* 95 (1990) 18577-18582.

660doi:10.1029/JD095iD11p18577.

661

662[2] R. Thalman, R. Volkamer, Temperature dependent absorption cross sections of O₂-O₂ collision pairs
663between 340 and 630 nm and at atmospherically relevant pressure, *Physical Chemistry Chemical*
664*Physics* 15 (37) (2013) 15371-15381. doi:10.1039/c3cp50968k.

665

666[3] T. Wagner, B. Dix, C. v. Friedeburg, U. Friess, S. Sanghavi, R. Sinreich, U. Platt, MAX-DOAS O₄
667measurements: A new technique to derive information on atmospheric aerosols-Principles and
668information content, *Journal of Geophysical Research (Atmospheres)* 109 (2004) D22205.

669doi:10.1029/2004JD004904.

670

671[4] U. Friess, P. S. Monks, J. J. Remedios, A. Rozanov, R. Sinreich, T. Wagner, U. Platt, MAX-DOAS
672O₄ measurements: A new technique to derive information on atmospheric aerosols: 2. Modeling studies,
673*Journal of Geophysical Research (Atmospheres)* 111 (2006) D14203. doi:10.1029/2005JD006618.

674

675[5] K. Clémer, M. Van Roozendael, C. Fayt, F. Hendrick, C. Hermans, G. Pinardi, R. Spurr, P. Wang,
676M. De Maziere, Multiple wavelength retrieval of tropospheric aerosol optical properties from
677MAXDOAS measurements in Beijing, *Atmospheric Measurement Techniques* 3 (4) (2010) 863-878.
678doi:10.5194/amt-3-863-2010.

679

680[6] R. Sinreich, A. Merten, L. Molina, R. Volkamer, Parameterizing radiative transfer to convert
681MAX-DOAS dSCDs into near-surface box-averaged mixing ratios, *Atmospheric Measurement*
682*Techniques* 6 (2013) 1521-1532. doi:10.5194/amt-6-1521-2013.

683

684[7] M. L. Melamed, A. O. Langford, J. S. Daniel, R. W. Portmann, H. L. Miller, C. S. Eubank, R.
685Schofield, J. Holloway, S. Solomon, Sulfur dioxide emission flux measurements from point sources
686using airborne near ultraviolet spectroscopy during the new England air quality study 2004, Journal of
687Geophysical Research: Atmospheres 113 (D2) (2008). doi:10.1029/2007JD008923.

688

689[8] S. Baidar, H. Oetjen, S. Coburn, B. Dix, I. Ortega, R. Sinreich, R. Volkamer, The CU Airborne
690MAX-DOAS instrument: vertical profiling of aerosol extinction and trace gases, Atmospheric
691Measurement Techniques 6 (3) (2013) 719-739. doi:10.5194/amt-6-719-2013.

692

693[9] R. Volkamer, S. Baidar, T. L. Campos, S. Coburn, J. P. DiGangi, B. Dix, E. W. Eloranta, T. K.
694Koenig, B. Morley, I. Ortega, B. R. Pierce, M. Reeves, R. Sinreich, S. Wang, M. A. Zondlo, P. A.
695Romashkin, Aircraft measurements of BrO, IO, glyoxal, NO₂, H₂O, O₂O₂ and aerosol extinction
696profiles in the tropics: comparison with aircraft-/ship-based in situ and lidar measurements,
697Atmospheric Measurement Techniques 8 (5) (2015) 2121-2148. doi:10.5194/amt-8-2121-2015.

698

699[10] S. Coburn, I. Ortega, R. Thalman, B. Blomquist, C. W. Fairall, R. Volkamer, Measurements of
700diurnal variations and eddy covariance (EC) fluxes of glyoxal in the tropical marine boundary layer:
701description of the fast LED-CE-DOAS instrument, Atmospheric Measurement Techniques 7 (10)
702(2014) 3579-3595. doi:10.5194/amt-7-3579-2014.

703[11] J. R. Acarreta, J. F. De Haan, P. Stammes, Cloud pressure retrieval using the O₂-O₂ absorption band
704at 477 nm, Journal of Geophysical Research (Atmospheres) 109 (2004) 5204.
705doi:10.1029/2003JD003915.

706

707[12] T. Wagner, J. P. Burrows, T. Deutschmann, B. Dix, C. von Friedeburg, U. Friess, F. Hendrick, K.
708Heue, H. Irie, H. Iwabuchi, Y. Kanaya, J. Keller, C. A. McLinden, H. Oetjen, E. Palazzi, A. Petritoli, U.
709Platt, O. Postylyakov, J. Pukite, A. Richter, M. van Roozendael, A. Rozanov, V. Rozanov, R. Sinreich,
710S. Sanghavi, F. Wittrock, Comparison of box-air-mass-factors and radiances for Multiple-Axis
711Differential Optical Absorption Spectroscopy (MAX-DOAS) geometries calculated from different
712UV/visible radiative transfer models, Atmospheric Chemistry and Physics 7 (7) (2007) 1809-1833.

713

714[13] C. D. Rodgers, Inverse Methods for Atmospheric Sounding: Theory and Practice, World Scientific,
715Singapore, 2000.

716

717[14] T. Wagner, T. Deutschmann, U. Platt, Determination of aerosol properties from MAX-DOAS
718observations of the Ring effect, Atmospheric Measurement Techniques 2 (2) (2009) 495-512.
719doi:10.5194/amt-2-495-2009.

720

721[15] H. Irie, H. Takashima, Y. Kanaya, K. F. Boersma, L. Gast, F. Wittrock, D. Brunner, Y. Zhou, M.
722Van Roozendael, Eight-component retrievals from ground-based MAX-DOAS observations,
723Atmospheric Measurement Techniques 4 (6) (2011) 1027-1044. doi:10.5194/amt-4-1027-2011.

724

725[16] T. Vlemmix, A. J. M. Piters, A. J. C. Berkhou, L. F. L. Gast, P. Wang, P. F. Levelt, Ability of the
726MAX-DOAS method to derive profile information for NO₂: can the boundary layer and free
727troposphere be separated?, Atmospheric Measurement Techniques 4 (12) (2011) 2659-2684.
728doi:10.5194/amt-4-2659-2011.

729

730[17] P. Zieger, E. Weingartner, J. Henzing, M. Moerman, G. de Leeuw, J. Mikkila, M. Ehn, T. Petaja, K.
731Clémer, M. van Roozendael, S. Yilmaz, U. Friess, H. Irie, T. Wagner, R. Shaiganfar, S. Beirle, A.
732Apituley, K. Wilson, U. Baltensperger, Comparison of ambient aerosol extinction coefficients obtained
733from in-situ, MAX-DOAS and lidar measurements at Cabauw, Atmospheric Chemistry and Physics 11
734(6) (2011) 2603-2624. doi:10.5194/acp-11-2603-2011.

735

736[18] H. Irie, T. Nakayama, A. Shimizu, A. Yamazaki, T. Nagai, A. Uchiyama, Y. Zaizen, S. Kagamitani,
737Y. Matsumi, Evaluation of max-doas aerosol retrievals by coincident observations using crds, lidar, and
738sky radiometer intsukuba, japan, Atmospheric Measurement Techniques 8 (7) (2015) 2775-115 2788.
739doi:10.5194/amt-8-2775-2015.

740

741[19] E. Spinei, A. Cede, J. Herman, G. H. Mount, E. Eloranta, B. Morley, S. Baidar, B. Dix, I. Ortega,
742T. Koenig, R. Volkamer, Ground-based direct-sun DOAS and airborne MAX-DOAS measurements of
743the collision induced oxygen complex, O₂O₂, absorption with significant pressure and temperature
744differences, Atmospheric Measurement Techniques 8 (2015) 793-809. doi:10.5194/amt-8-793-2015.

745

746[20] J. Remmers, T. Wagner, Azimuthal variability of trace gases and aerosols measured during the
747MADCAT campaign in summer 2013 in Mainz, Germany, Presentation at the 7th International DOAS
748Workshop, Brussels, 6-8 July 2015.

749

750[21] L. K. Berg, J. D. Fast, J. C. Barnard, S. P. Burton, B. Cairns, D. Chand, J. M. Comstock, S.
751Dunagan, R. A. Ferrare, C. J. Flynn, J. W. Hair, C. A. Hostetler, J. Hubbe, A. Je_erson, R. Johnson, E.
752I. Kassianov, C. D. Kluzek, P. Kollias, K. Lamer, K. Lantz, F. Mei, M. A. Miller, J. Michalsky, I.
753Ortega, M. Pekour, R. R. Rogers, P. B. Russell, J. Redemann, A. J. Sedlacek, M. Segal-Rosenheimer,
754B. Schmid, J. E. Shilling, Y. Shinozuka, S. R. Springston, J. M. Tomlinson, M. Tyrrell, J. M. Wilson, R.
755Volkamer, A. Zelenyuk, C. M. Berkowitz, The Two-Column Aerosol Project: Phase I Overview and
756Impact of Elevated Aerosol Layers on Aerosol Optical Depth, *Journal of Geophysical Research: Atmospheres* (2015). doi:10.1002/2015JD023848.

758

759[22] I. Ortega, T. Koenig, R. Sinreich, D. Thomson, R. Volkamer, The CU 2-D-MAX-DOAS instrument
760- Part 1: Retrieval of 3-D Distributions of NO₂ and azimuth-dependent OVOC ratios, *Atmospheric
761Measurement Techniques* 8 (6) (2015) 2371-2395. doi:10.5194/amt-8-2371-2015.

762

763[23] U. Platt, J. Stutz, *Differential Optical Absorption Spectroscopy: Principles and Applications*,
764Springer Verlag, Heidelberg, 2008.

765

766[24] C. Fayt, M. Van Roozendael, WinDOAS 2.1, software user manual, Belgian Institute for Space
767Aeronomy, Brussels, Belgium, available at:
768<http://uv-vis.aeronomie.be/software/windoas/windoas-sum-210b.pdf> (last access: 29 May 2012) (2001).

769

770[25] K. Bogumil, J. Orphal, T. Homann, S. Voigt, P. Spietz, O. Fleischmann, A. Vogel, M. Hartmann,
771H. Kromminga, H. Bovensmann, J. Frerick, J. Burrows, Measurements of molecular absorption spectra
772with the SCIAMACHY pre-flight model: instrument characterization and reference data for
773atmospheric remote-sensing in the 230-2380 nm region, *Journal of Photochemistry and Photobiology
774A-Chemistry* 157 (2-3) (2003) 167-184. doi:10.1016/S1010-6030(03)00062-5.

775

776[26] A. Vandaele, C. Hermans, P. Simon, M. Carleer, R. Colin, S. Fally, M. Merienne, A. Jenouvrier, B.
777Coquart, Measurements of the NO₂ absorption cross-section from 42 000 cm⁻¹ to 10 000 cm⁻¹
778(238-1000 nm) at 220 K and 294 K, *Journal of Quantitative Spectroscopy & Radiative Transfer* 59
779(3-5) (1998) 171-184. doi:10.1016/S0022-4073(97)00168-4.

780

781[27] L. Rothman, I. Gordon, Y. Babikov, A. Barbe, D. C. Benner, P. Bernath, M. Birk, L. Bizzocchi, V.
782Boudon, L. Brown, A. Campargue, K. Chance, E. Cohen, L. Coudert, V. Devi, B. Drouin, A. Fayt,

783J.-M. Flaud, R. Gamache, J. Harrison, J.-M. Hartmann, C. Hill, J. Hodges, D. Jacquemart, A. Jolly, J.
784Lamouroux, R. L. Roy, G. Li, D. Long, O. Lyulin, C. Mackie, S. Massie, S. Mikhailyko, H. Müller, O.
785Naumenko, A. Nikitin, J. Orphal, V. Perevalov, A. Perrin, E. Polovtseva, C. Richard, M. Smith, E.
786Starikova, K. Sung, S. Tashkun, J. Tennyson, G. Toon, V. Tyuterev, G. Wagner, The HITRAN2012
787molecular spectroscopic database, Journal of Quantitative Spectroscopy and Radiative Transfer 130
788(2013) 4 - 50, HITRAN2012g special issue. doi:10.1016/j.jqsrt.2013.07.002.

789

790[28] R. Volkamer, P. Spietz, J. Burrows, U. Platt, High-resolution absorption cross-section of glyoxal in
791the UV-vis and IR spectral ranges, Journal of Photochemistry and Photobiology A-Chemistry 172 (1)
792(2005) 35-46. doi:10.1016/j.jphotochem.2004.11.011.

793

794[29] R. Meller, G. Moortgat, Temperature dependence of the absorption cross sections of formaldehyde
795between 223 and 323 K in the wavelength range 225-375 nm, Journal of Geophysical
796Research-Atmospheres 105 (D6) (2000) 7089-7101. doi:10.1029/1999JD901074.

797

798[30] O. C. Fleischmann, M. Hartmann, J. P. Burrows, J. Orphal, New ultraviolet absorption
799cross-sections of bro at atmospheric temperatures measured by time-windowing fourier transform
800spectroscopy, Journal of Photochemistry and Photobiology A: Chemistry 168 (12) (2004) 117-132. doi:
80110.1016/j.jphotochem.2004.03.026.

802

803[31] S. Kraus, A framework design for doas (2006).

804

805[32] J. Grainger, J. Ring, Anomalous Fraunhofer line profiles, Nature 193 (4817) (1962) 762.

806doi:10.1038/193762a0.

807

808[33] C. Hermans, Measurement of absorption cross sections and spectroscopicmolecular parameters:
809O₂ and its collisional induced absorption, available at: <http://spectrolab.aeronomie.be/o2.htm> (last
810access: 29 May 2012), 2002.

811

812[34] J. W. Hair, C. A. Hostetler, A. L. Cook, D. B. Harper, R. A. Ferrare, T. L. Mack, W. Welch, L. R.
813Izquierdo, F. E. Hovis, Airborne high spectral resolution lidar for profiling aerosol optical properties,
814Appl. Opt. 47 (36) (2008) 6734-6752. doi:10.1364/AO.47.006734.

815

816[35] C. J. Grund, E. W. Eloranta, University of Wisconsin high spectral resolution lidar, Optical
817Engineering 30 (1) (1991) 6-12. doi:10.1117/12.55766.

818[36] D. Muller, C. A. Hostetler, R. A. Ferrare, S. P. Burton, E. Chemyakin, A. Kolgotin, J. W. Hair, A.
819L. Cook, D. B. Harper, R. R. Rogers, R. W. Hare, C. S. Cleckner, M. D. Oblard, J. Tomlinson, L. K.
820Berg, B. Schmid, Airborne Multiwavelength High Spectral Resolution Lidar (HSRL-2) observations
821during TCAP 2012: vertical profiles of optical and microphysical properties of a smoke/urban haze
822plume over the northeastern coast of the US, Atmospheric Measurement Techniques 7 (10) (2014)
8233487-3496. doi:10.5194/amt-7-3487-2014.

824

825[37] B. A. Bodhaine, N. B. Wood, E. G. Dutton, J. R. Slusser, On Rayleigh Optical Depth Calculations,
826Journal of Atmospheric and Oceanic Technology 16 (1999) 1854.
827doi:10.1175/1520-0426(1999)016<1854:ORODC>2.0.CO;2.

828

829[38] L. Harrison, J. Michalsky, Objective algorithms for the retrieval of optical depths from
830ground-based measurements, Appl. Opt. 33 (22) (1994) 5126-5132. doi:10.1364/AO.33.005126.

831

832[39] B. Holben, T. Eck, I. Slutsker, D. Tanr, J. Buis, A. Setzer, E. Vermote, J. Reagan, Y. Kaufman, T.
833Nakajima, F. Lavenu, I. Jankowiak, A. Smirnov, AERONET a federated instrument network and data
834archive for aerosol characterization, Remote Sensing of Environment 66 (1) (1998) 1 - 16. doi:
83510.1016/S0034-4257(98)00031-5.

836

837[40] T. Deutschmann, S. Beirle, U. Friess, M. Grzegorski, C. Kern, L. Kritten, U. Platt, C.
838Prados-Roman, J. Pukite, T. Wagner, B. Werner, K. Pfeilsticker, The Monte Carlo atmospheric
839radiative transfer model McArtim: Introduction and validation of Jacobians and 3D features, Journal of
840Quantitative Spectroscopy & Radiative Transfer 112 (6) (2011) 1119-1137.
841doi:10.1016/j.jqsrt.2010.12.009.

842

843[41] E. Kassianov, J. Barnard, C. Flynn, L. Riihimaki, J. Michalsky, G. Hodges, Areal-averaged
844spectral surface albedo from ground-based transmission data alone: Toward an operational retrieval,
845Atmosphere 5 (3) (2014) 597. doi:10.3390/atmos5030597.

846

847[42] R. B. A. Koelemeijer, J. F. de Haan, P. Stammes, A database of spectral surface reectivity in the
848range 335772 nm derived from 5.5 years of GOME observations, Journal of Geophysical Research:
849Atmospheres 108 (D2) (2003), 4070. doi:10.1029/2002JD002429.

850

851[43] O. Dubovik, B. Holben, T. F. Eck, A. Smirnov, Y. F. Kaufman, M. D. King, D. Tanre, I. Slutsker,
852Variability of absorption and optical properties of key aerosol types observed in worldwide locations,
853Journal of the Atmospheric Sciences 59 (2002) 590-608.
854doi:10.1175/1520-0469(2002)059<0590:VOAAOP>2.0.CO;2.

855

856[44] A. H. Goldstein, C. D. Koven, C. L. Heald, I. Y. Fung, Biogenic carbon and anthropogenic
857pollutants combine to form a cooling haze over the southeastern United States, Proceedings of the
858National Academy of Sciences 106 (22) (2009) 8835-8840. doi:10.1073/pnas.0904128106.

859

860[45] D. M. Winker, J. L. Tackett, B. J. Getzewich, Z. Liu, M. A. Vaughan, R. R. Rogers, The global
8613-D distribution of tropospheric aerosols as characterized by CALIOP, Atmospheric Chemistry and
862Physics 13 (6) (2013) 3345-3361. doi:10.5194/acp-13-3345-2013.

863

864[46] O. Boucher, D. Randall, P. Artaxo, C. Bretherton, G. Feingold, P. Forster, V.-M. Kerminen, Y.
865Kondo, H. Liao, U. Lohmann, P. Rasch, S.K. Satheesh, S. Sherwood, B. Stevens and X.Y. Zhang,
866Clouds and Aerosols. In: Climate Change 2013: The Physical Science Basis. Contribution of Working
867Group I to the Fifth Assessment Report of the Intergovernmental Panel on Climate Change [Stocker,
868T.F., D. Qin, G.-K. Plattner, M. Tignor, S.K. Allen, J. Boschung, A. Nauels, Y. Xia, V. Bex and P.M.
869Midgley (eds.)]. (2013), Cambridge University Press, Cambridge, United Kingdom and New York,
870NY, USA.

871

872[47] N. Papagiannopoulos, L. Mona, L. Alados-Arboledas, V. Amiridis, H. Baars, I. Binietoglou, D.
873Bortoli, G. D'Amico, A. Giunta, J. L. Guerrero-Rascado, A. Schwarz, S. Pereira, N. Spinelli, U.
874Wandinger, X. Wang, G. Pappalardo, Calipso climatological products: evaluation and suggestions from
875earlinet, Atmospheric Chemistry and Physics Discussions 15 (21) (2015) 31197-31246.
876doi:10.5194/acpd-15-31197-2015.

877

878[48] B. Dix, S. Baidar, J. F. Bresch, S. R. Hall, K. S. Schmidt, S. Wang, R. Volkamer, Detection of
879iodine monoxide in the tropical free troposphere, Proceedings of the National Academy of Sciences of
880the United States of America 110 (6) (2013) 2035-2040. doi:10.1073/pnas.1212386110.

881

882[49] S. Wang, J. A. Schmidt, S. Baidar, S. Coburn, B. Dix, T. K. Koenig, E. Apel, D. Bowdalo, T. L.
883Campos, E. Eloranta, M. J. Evans, J. P. DiGangi, M. A. Zondlo, R.-S. Gao, J. A. Haggerty, S. R. Hall,
884R. S. Hornbrook, D. Jacob, B. Morley, B. Pierce, M. Reeves, P. Romashkin, A. ter Schure, R.
885Volkamer, Active and widespread halogen chemistry in the tropical and subtropical free troposphere,
886Proceedings of the National Academy of Sciences 112 (30) (2015) 9281-9286.
887doi:10.1073/pnas.1505142112.

888

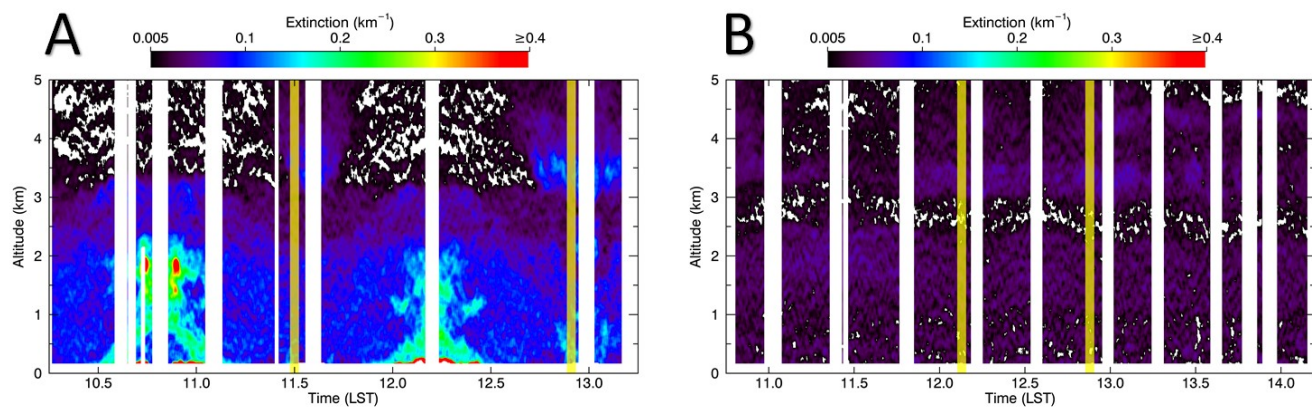
889[50] I. Ortega, S. Coburn, L.K. Berg, K. Lantz, J. Michalsky, R. Ferrare, J. Hair, C. Hostetler, R.
890Volkamer, The CU 2D-MAX-DOAS instrument - part 2: Raman Scattering Probability Measurements
891and Retrieval of Aerosol Optical Properties, Atmospheric Measurement Techniques Discussions (2016)
892doi:10.5194/amt-2015-385.

893

894

Supplementary figures

895

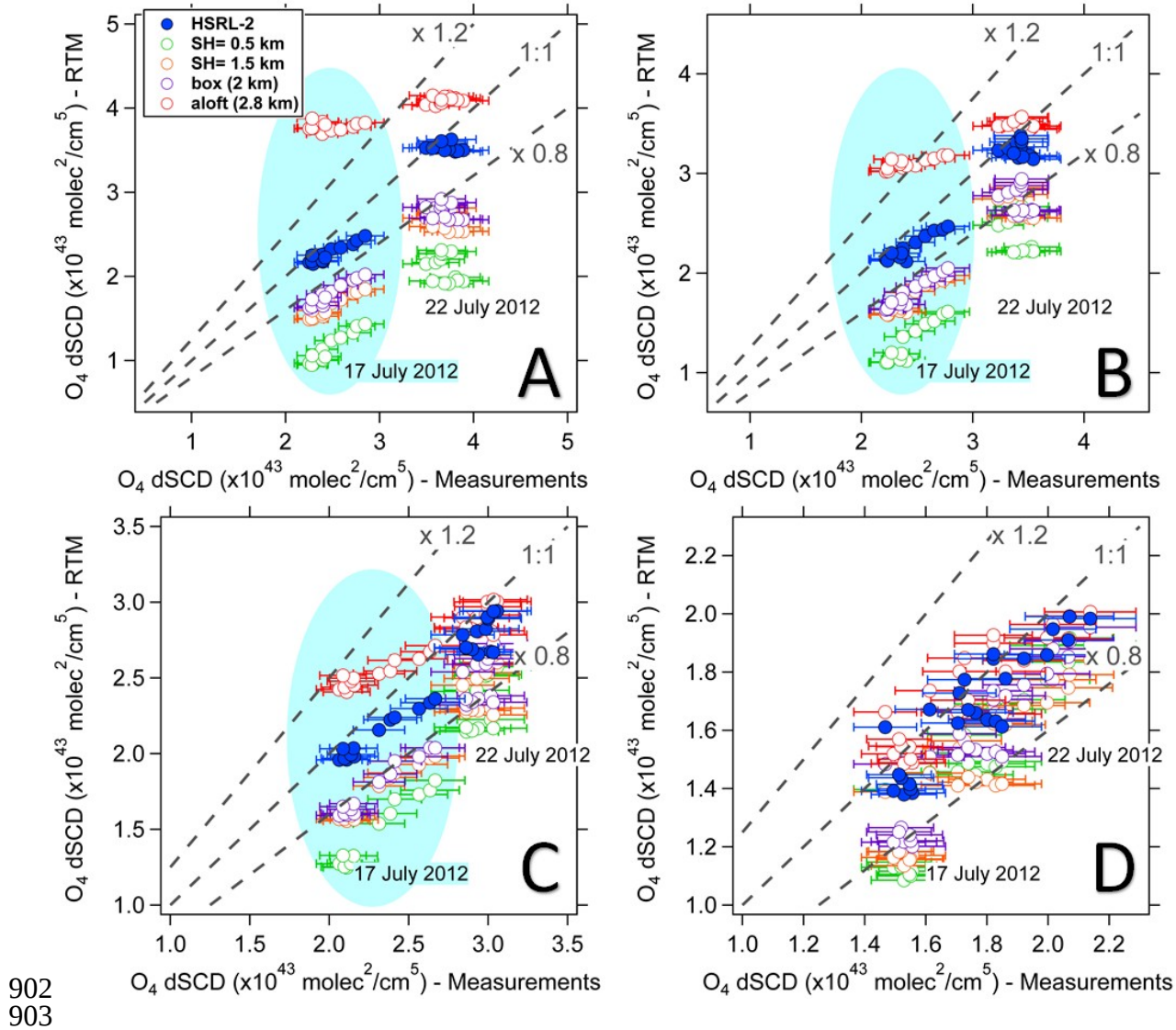


896

897 Figure S1: Aerosol extinction (532 nm) curtain plots on 17 (A) and 22 (B) July 2012. Both plots are
898 shown on the same scale to contrast the difference in extinction on both days. The yellow vertical lines
899 represent the average time during the overpasses above the TCAP ground site.

900

901



904Figure S2: Comparison of O_4 dSCDs measured and simulated at 360 nm for the elevation angles of 3°
905(A), 6° (B), 10° (C), and 20° (D). Note that the magnitude of the axis are different for each elevation
906angle. The light blue shaded oval represents values from 17 July, which are easily identified for low
907elevation angles ($\leq 10^\circ$). For the elevation angle of 20° there is not an apparent split in the O_4 dSCDs
908for the different days. The O_4 dSCD error bars in the measurements represent the 7 % described in
909Section 2.1

910

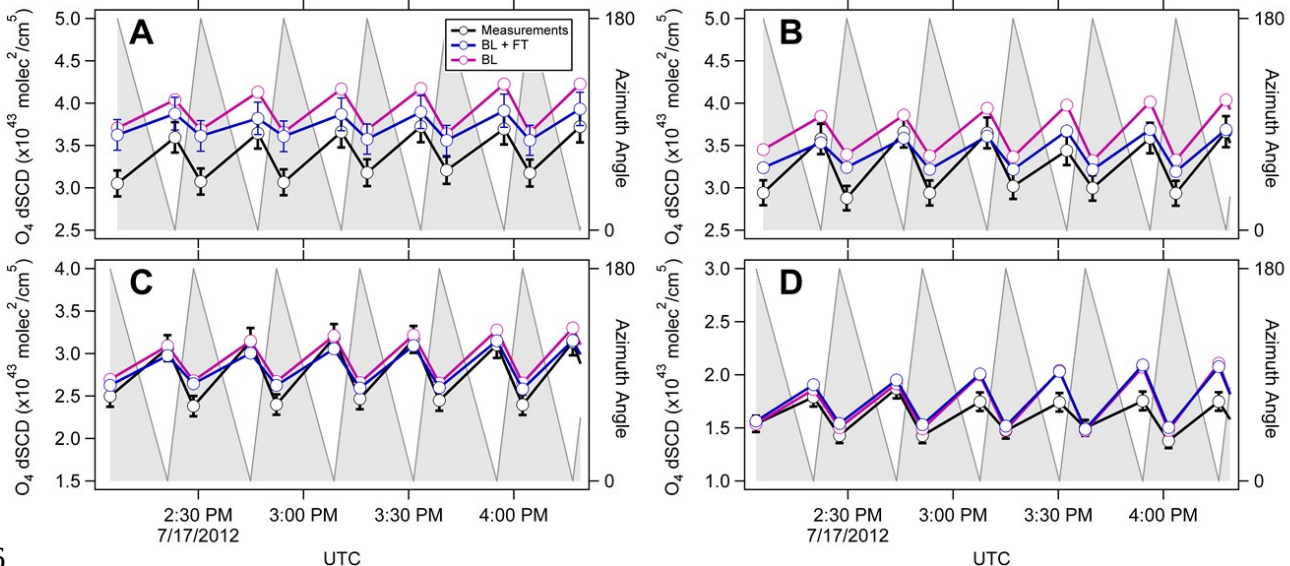
911

912

913

914

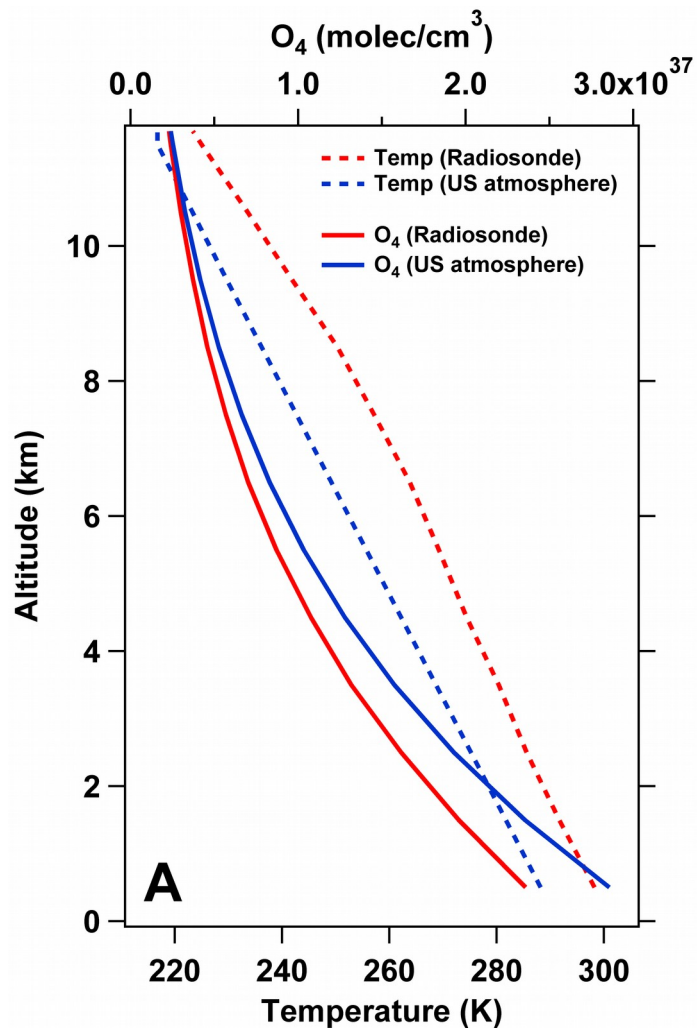
915



916

917Figure S3. Time series of O_4 dSCDs measured on 17 July 2012 during the HSRL-2 overpass, and
918simulated using the aerosol extinction from HSRL-2 below 2 km and removing aerosol aloft at 477 nm
919for the EAs of (A) 3°, (B) 6°, (C) 10°, and (D) 20°. The gray line indicates the viewing angle (0 =
920north; 180 = south).

921



922

923Figure S4. Comparison of the temperature (dotted line) and O_4 concentration profiles (continuous line)
 924using the co-located radiosonde measurements (red) and U.S standard atmosphere (blue). The example
 925shown is from 17 July 2012. If the U.S standard atmosphere is used the O_4 concentration profile is
 926overestimated, hence the O_4 dSCDs are overestimated.